antibodies and analyzed by flow cytometry (Fig. 2). $CD34^-KSL$ cells accounted for 0.005 ± 0.002 (mean ± standard deviation [SD], n = 4) of BM cells as reported [20–22] and accounted for 0.0004 ± 0.0004 (n = 4) of spleen cells. On the other hand, $CD34^+KSL$ cells accounted for 0.14 ± 0.02 (n = 4) and 0.004 ± 0.001 (n = 4) of BM and spleen cells, respectively. To examine the function of $CD34^-$ or $CD34^+KSL$ spleen cells, 100 cells from each fraction were transplanted into each of a group of lethally irradiated mice. As in BM, $CD34^-KSL$ cells, but not $CD34^+KSL$ cells in the spleen, were enriched in long-term repopulating activity (Supplementary Figure E2; online only, available at www.exphem.org). We decided to characterize spleen HSCs further by using $CD34^-KSL$ cells as an HSC-enriched fraction.

Colony-forming activity in BM and spleen $CD34^-KSL$ cells

As shown in Supplementary Figure E3 (online only, available at www.exphem.org), >90% of BM $CD34^-KSL$ cells formed colonies in vitro as reported [23]. Although their colony-forming efficiency seemed slightly lower, >80% of spleen $CD34^-KSL$ cells formed colonies in vitro. Colony-forming units with differentiation potential for all neutrophil, macrophage, erythrocyte, and megakaryocyte lineages, which is possibly another aspect of LTRC activity [23], were similarly detected in BM and spleen $CD34^-KSL$ cells. These data support the concept that $CD34^-KSL$ cells are similarly enriched in both BM and spleen HSCs of adult mice.

Competitive repopulation with BM and spleen $CD34^-KSL$ cells

Competitive repopulating assays were performed on BM or spleen $CD34^-KSL$ cells. Figure 3 shows data from transplantation of 10 $CD34^-KSL$ cells and of single such cells. After 10 BM or spleen $CD34^-KSL$ cells were transplanted, a variety of levels of percent chimerism was observed among individual recipient mice (Fig. 3A). Long-term reconstitution levels achieved by 10 spleen $CD34^-KSL$ cells did not significantly differ on average from those achieved by 10 BM $CD34^-KSL$ cells (Fig. 3A). In order to compare self-renewal potential, secondary transplantation was performed with BM cells pooled from all primary recipient mice. After secondary transplantation, levels of percent chimerism did not significantly differ between recipients of BM and spleen $CD34^-KSL$ cells (Fig. 3B). These data show that repopulating and self-renewal potentials are similar in BM and spleen $CD34^-KSL$ cells.

To confirm that the engraftment rates of LRTCs are also similar between BM and spleen $CD34^-KSL$ cells, single-cell transplantation was performed. Transplantation of single BM or spleen $CD34^-KSL$ cells resulted in long-term reconstitution in 9 of 29 or 7 of 29 recipient mice, respectively (Fig. 3C). Based on data from transplantation with 10 cells and single cells, we roughly estimated the frequency of LTRCs. The frequency of LTRCs in BM $CD34^-KSL$ cells was about one in three cells, consistent with our previous observations [21], while that in spleen $CD34^-KSL$ cells was

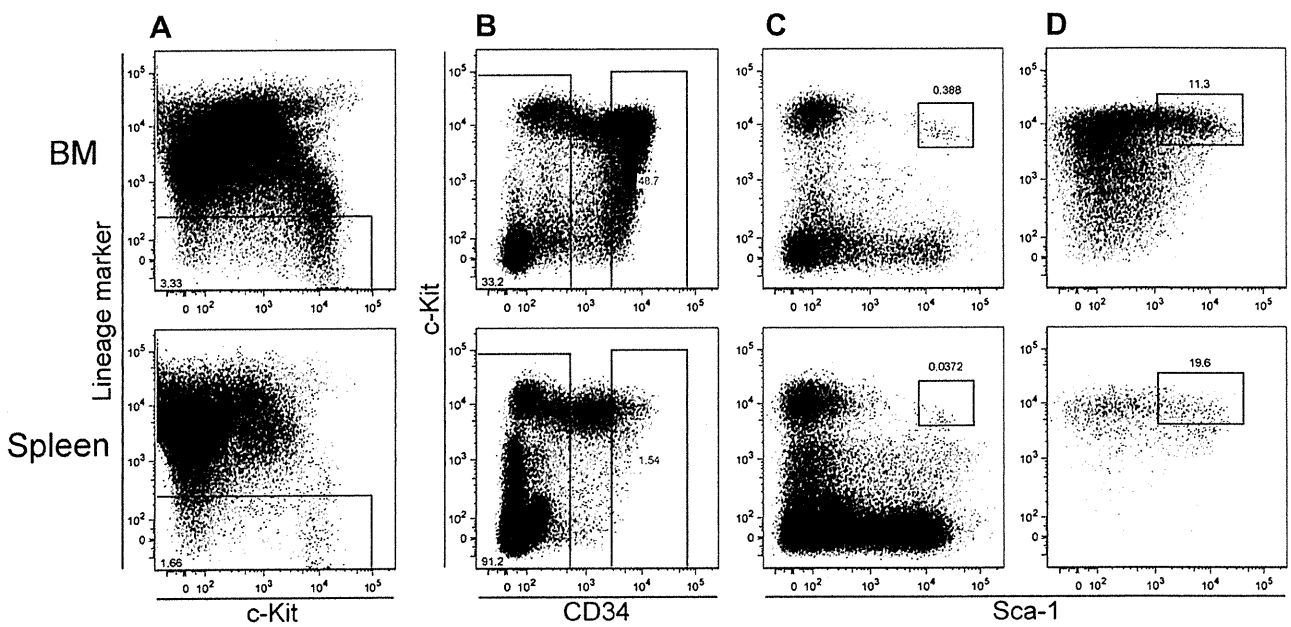

Figure 2. $CD34^-KSL$ cells in BM and spleen. Lineage-depleted BM or spleen cells were stained with antibodies and analyzed on a flow cytometer. The upper and lower panels show BM analysis and spleen analysis, respectively. (**A**) Dot plots display expression of c-Kit and lineage markers with square gates for lineage-negative cells. (**B**) Dot plots display expression of CD34 and c-Kit in lineage-negative cells with square gates for $CD34^{-/low}$ or $CD34^+$ lineage-negative cells. (**C**) Dot plots display expression of Sca-1 and c-Kit in $CD34^{-/low}$ lineage-negative cells with square gates for $CD34^-KSL$ cells. (**D**) Dot plots display expression of Sca-1 and c-Kit in $CD34^+$ lineage-negative cells with square gates for $CD34^+KSL$ cells.

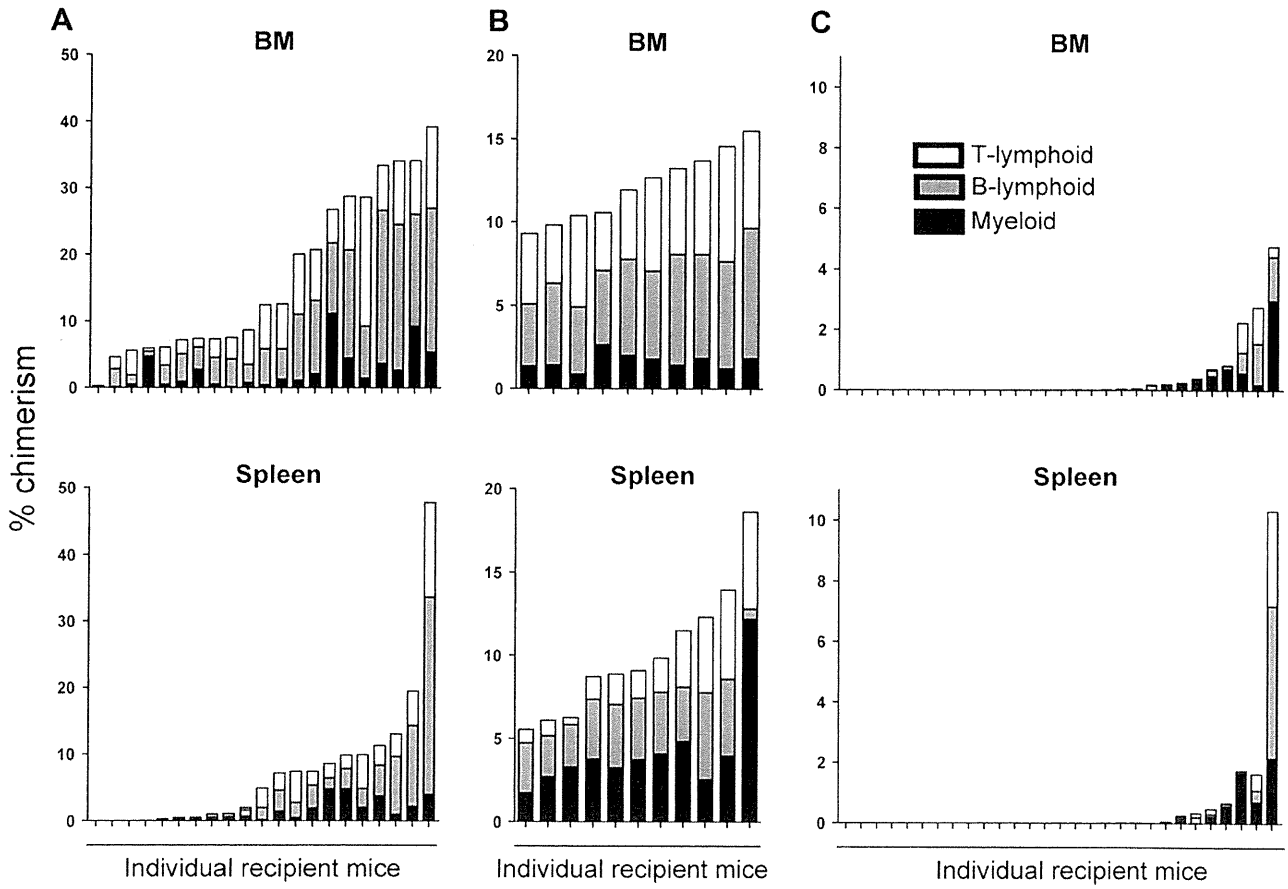

Figure 3. Long-term reconstitution by 10 BM or spleen CD34$^-$KSL cells or by individual such cells. (**A**) 10 CD34$^-$KSL cells from BM or spleen were transplanted into each of 21 lethally irradiated mice, together with 2 × 10^5 BM cells. Recipient mice were analyzed 16 weeks after transplantation. Each column represents percent chimerism (consisting of myeloid, B-lymphoid, and T-lymphoid lineages). Percent chimerism was 16.7% ± 12.3% (mean ± SD, n = 21) for BM CD34$^-$KSL cells and 9.0% ± 11.3% (n = 17) for spleen CD34$^-$KSL cells. (**B**) Secondary transplantation was performed with pooled bone marrow cells from all primary recipient mice. Recipient mice were analyzed 13 weeks after transplantation. Percent chimerism was 12.3% ± 2.1% (n = 10) for cells derived from BM CD34$^-$KSL cells and 9.8% ± 4.0% (n = 11) for cells derived from spleen CD34$^-$KSL cells. (**C**) Single CD34$^-$KSL cells from BM or spleen were transplanted into each of 30 lethally irradiated mice, together with 2 × 10^5 BM cells. Recipient mice were analyzed 12 weeks after transplantation. Each column represents percent chimerism. One mouse in each group died before analysis. Of 29 recipient mice, 9 and 7 were reconstituted with single BM or spleen CD34$^-$KSL cells, respectively. Recipient mice with >0.1% chimerism for one or more lineages are shown.

about one in five cells. These data did not permit statistical analysis. If a large number of single cells were transplanted or limiting dilution type of experiments were performed, a significant difference in frequency of LTRCs between BM and spleen CD34$^-$KSL cells would be obtained. However, such a difference should be only trivial. Predominant lymphoid reconstitution, seen after transplantation with whole spleen cells (Supplementary Figure E1; online only, available at www.exphem.org), was never detected after transplantation with spleen CD34$^-$KSL cells (Fig. 3). These data support the possibility that lymphoid repopulating cells other than HSCs are present in the spleen.

Spleen HSCs differ from circulating HSCs

As blood flow through the spleen is abundant, transiently circulating HSCs could have been detected as spleen HSCs. In order to address this issue, a parabiosis model was used in which cross-circulation was established in B6-Ly5.1:B6-Ly5.2 mouse pairs. Five pairs of mice could be analyzed at 7 or 14 weeks of parabiosis (Fig. 4). In B6-Ly5.1 mice, 49.4% ± 4.4% (mean ± SD, n = 5) of peripheral blood cells were replaced by Ly5.2 cells. In B6-Ly5.2 mice, 39.2% ± 11.4% (mean ± SD, n = 5) of peripheral blood cells were replaced by Ly5.1 cells. These data confirmed near-equal mixing of peripheral blood in parabiosis [17]. All the following figures were calculated on the same basis. In B6-Ly5.1 mice, 20.4% ± 8.8% of whole BM cells were replaced by Ly5.2 cells. In B6-Ly5.2 mice, 20% ± 14.0% of whole BM cells were replaced by Ly5.1 cells. Interestingly, more cells were replaced by partner-derived cells in the spleen: In B6-Ly5.1 mice, 44.9% ± 7.1% of whole spleen cells were replaced by Ly5.2 cells, and in B6-Ly5.2 mice,

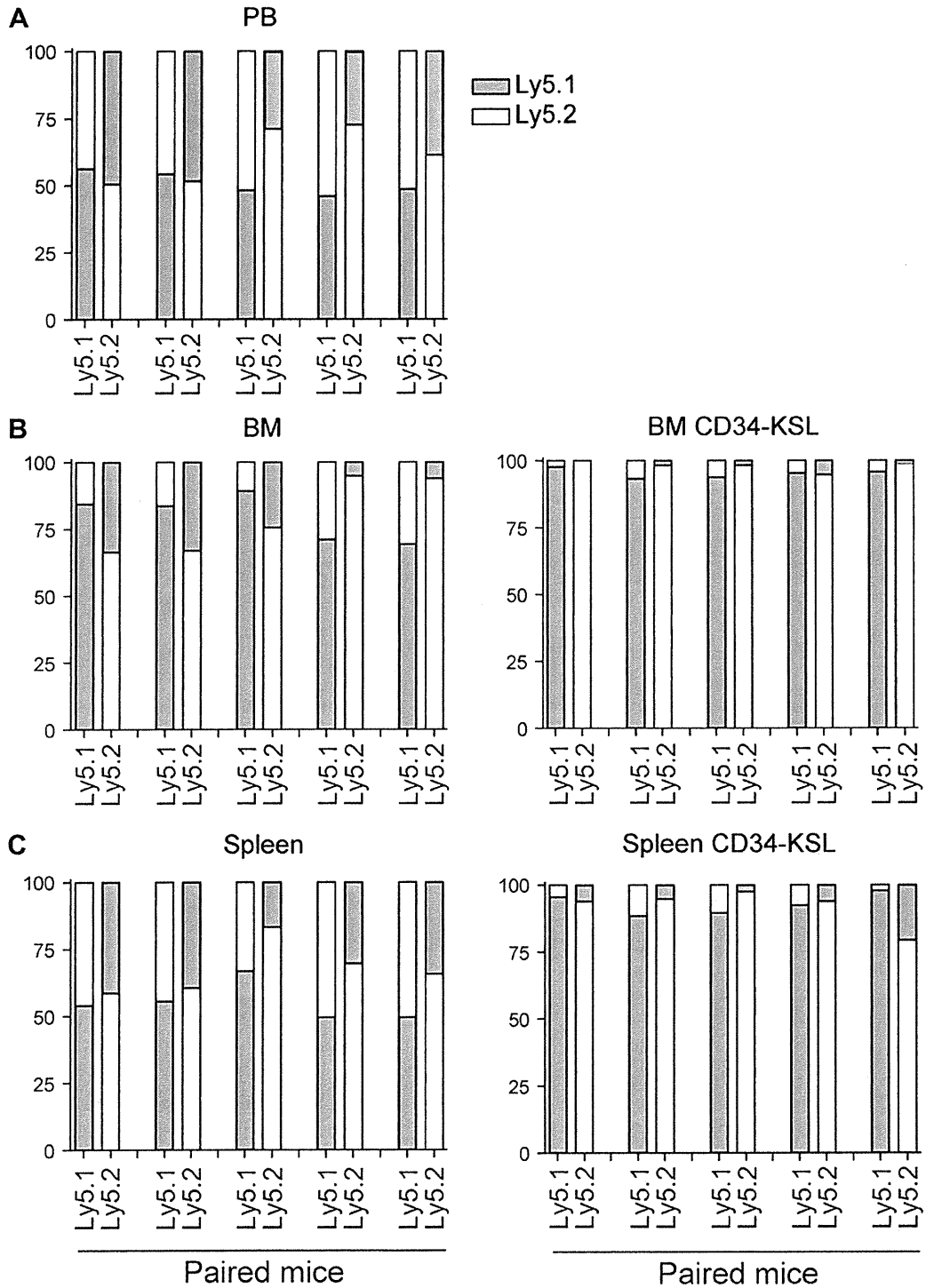

Figure 4. Analysis of parabiotic mice. (**A**) Peripheral blood cells of paired mice were analyzed for endogenous and partner-derived cells. (**B**) Whole BM cells (left panel) and BM CD34$^-$KSL cells (right panel) of paired mice were analyzed for endogenous and partner-derived cells. (**C**) Whole spleen cells (left panel) and spleen CD34$^-$KSL cells (right panel) of paired mice were analyzed for endogenous and partner-derived cells. B6-Ly5.1 mice were paired with B6-Ly5.2 mice. The pairs of mice were numbered 1-5 from left to right. Three pairs of mice (nos. 1, 2, and 3) were analyzed at 7 weeks of parabiosis. Two pairs of mice (nos. 4 and 5) were analyzed at 14 weeks of parabiosis. Pair no. 4 consisted of two male mice. The remaining pairs each consisted of two female mice.

32.5% ± 9.7% of whole spleen cells were replaced by Ly5.1 cells. These data show that, in parabiotic settings, a proportion of whole BM cells is exchangeable with cells from the circulation, and that most whole spleen cells become indistinguishable from peripheral blood cells after a certain interval.

With respect to the HSC population in parabiosis, significantly fewer cells were replaced by partner-derived cells. In B6-Ly5.1 mice, 6.6% ± 3.0% of BM CD34$^-$KSL cells and 8.6% ± 4.2% of spleen CD34$^-$KSL cells were replaced by Ly5.2 cells. In B6-Ly5.2 mice, 2.4% ± 1.7% of BM CD34$^-$KSL cells and 9.2% ± 6.4% of spleen CD34$^-$KSL cells were replaced by Ly5.2 cells. In contrast to the good numbers of unfractionated cells in BM and spleen that exchange places with their circulating counterparts, only small proportions of HSCs in BM and spleen exchange places with circulating HSCs. These data overall suggest that most spleen HSCs are long-term residents in the spleen.

Cell-cycle analysis of BM and spleen CD34$^-$KSL cells

Most adult HSCs are considered to be quiescent at any one time [24]. BM and spleen CD34$^-$KSL cells were stained with pyronin Y and were analyzed by flow cytometry (Fig. 5A). Pyronin Y^{low} cells were considered to be in the G_0 phase of the cell cycle (G_0 cells). Figure 5A shows representative data for G_0 cells among BM or spleen CD34$^-$KSL cells. G_0 cells accounted for 97.9% ± 1.5% (mean ± SD, n = 8) of BM CD34$^-$KSL cells, or 90.9 ± 5.2 (n = 8) of spleen CD34$^-$KSL cells. Paired *t*-testing showed significant differences between the two groups ($p = 0.0015$). These data suggest that spleen CD34$^-$KSL cells are more frequently in cycle than are BM CD34$^-$KSL cells.

To compare cell-cycle kinetics between BM and spleen CD34$^-$KSL cells, in vivo BrdU labeling was performed (Supplementary Figure E4; online only, available at www.exphem.org). The mean turnover time has been defined as the time point when BrdU-negative cells compose 37% of the cells analyzed and the 50% turnover time ($t_{1/2}$) has been defined as the time point when BrdU-negative cells compose 50% of the cells analyzed [25]. As shown in Figure 5B, the $t_{1/2}$ turned out to be approximately 17 days or 9 days for BM or spleen CD34$^-$KSL cells, respectively. The mean turnover time of BM CD34$^-$KSL cells was estimated to be approximately 25 days, consistent with previous observations [20,25]. In contrast, the mean turnover time of spleen CD34$^-$KSL cells was estimated to be approximately 13 days. The mean G_0 time was defined as (mean turnover time) minus (mean cell cycle time) when the G_0 concept was originally proposed by Lajtha [26]. The mean cell cycle time in HSCs is not yet determined precisely. The mean cell cycle time is presumably much shorter than the mean turnover time in HSCs, and cycling time does not differ between BM and spleen HSCs. The difference in the mean turnover time should arise largely from the difference in the mean G_0 time. These data show that spleen CD34$^-$KSL cells cycle almost twice as often as do BM CD34$^-$KSL cells.

Of interest was to know whether cell cycling in BM or spleen HSCs is determined cell intrinsically or cell extrinsically. To assess this, lethally irradiated mice were transplanted with BM or spleen cells. Mice were analyzed 12 months after transplantation. Mice were given BrdU for 1 week. BrdU uptake by CD34$^-$KSL cells was analyzed with Arrayscan in this series of experiments to permit reduction in the number of cells required for analysis. Analysis of BM or spleen CD34$^-$KSL cells from normal mice showed that spleen CD34$^-$KSL cells entered the cell cycle more frequently than did BM CD34$^-$KSL cells (Supplementary Figure E5A; online only, available at www.exphem.org), consistent with data from flow cytometric analysis (Supplementary Figure E4; online only, available at www.exphem.org). In reconstituted mice, regardless of the sources of donor HSCs, spleen CD34$^-$KSL cells were in cycle more frequently than were BM CD34$^-$KSL cells (Supplementary Figure E5B, C; online only, available at www.exphem.org). These data suggest organ-specific regulation for HSC cycling.

Discussion

This is the first study to show that spleen HSCs are phenotypically and functionally similar to BM HSCs. Data from both CRU assays (Fig. 1) and phenotypic analysis combined with reconstitution assays (Figs. 2, 3) showed that the frequency of HSCs in the spleen is significantly lower than that in the BM. However, data from both MAS estimation and single-cell transplantation (Fig. 3) showed that stem cell activity per cell is similar between BM and spleen HSCs. The functional similarity of BM and spleen HSCs raised the possibility that they interchange sites via the circulation. Parabiosis data (Fig. 4) suggested that most BM HSCs and spleen HSCs are long-term residents in each organ.

This study suggests that G_0 length differs between BM and spleen HSCs. Data from both pyronin Y staining and BrdU-uptake analysis (Fig. 5) indicate that spleen HSCs enter the cell cycle more frequently than do HSCs. The mean turnover time of BM HSCs was estimated to be about twice as long as that in spleen HSCs, suggesting that quiescence in BM HSCs is longer than in spleen HSCs. Interestingly, this was the case for BM and spleen HSCs in mice that had previously been reconstituted with BM or spleen cells (Supplementary Figure E5; online only, available at www.exphem.org). The duration of quiescence in HSCs might be regulated in an organ-specific manner. These data support the concept that the maintenance of quiescence in HSCs is a function of the HSC niche. Recently, the cell cycle of circulating HSCs was analyzed; BrdU uptake kinetics were reportedly similar in BM and PB HSCs

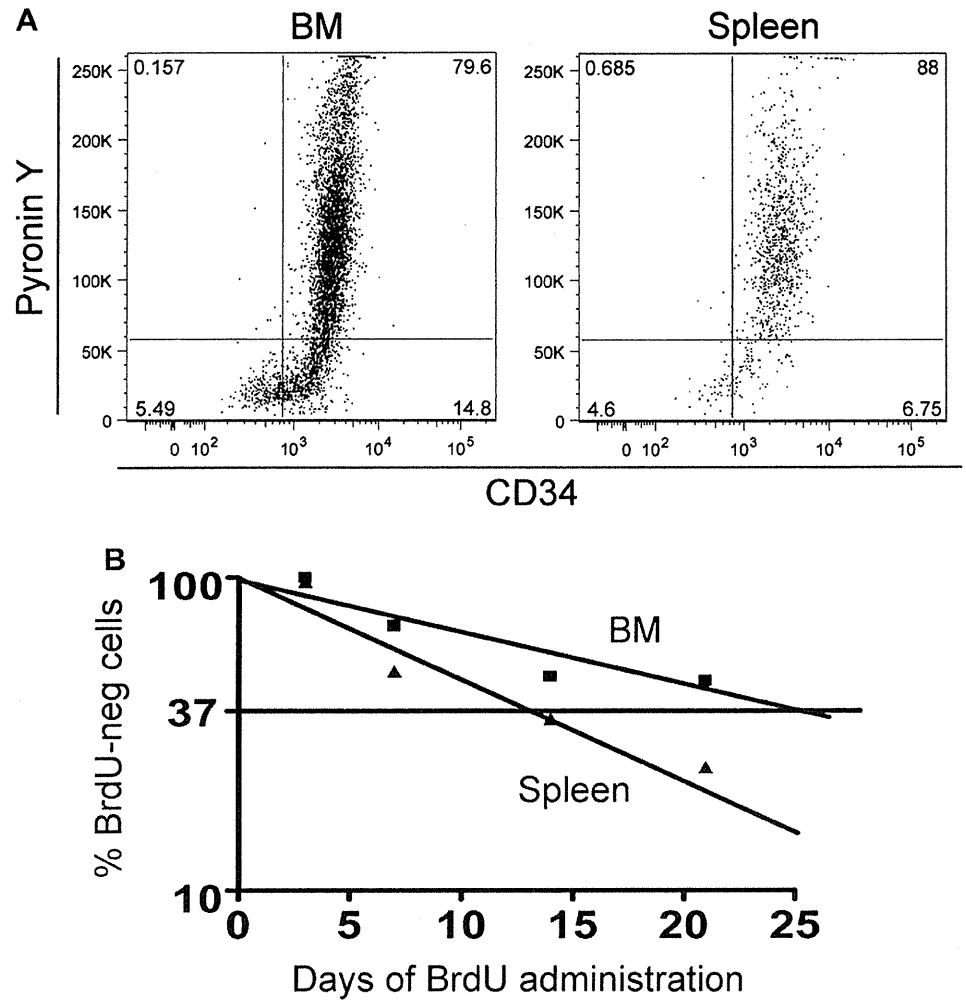

Figure 5. Cell-cycle analysis for BM or spleen CD34$^-$KSL cells. (**A**) CD34$^-$KSL cells were stained with pyronin Y. The representative flow cytometry profiles show CD34 expression and pyronin Y staining intensity in BM and spleen KSL cells. (**B**) The semi-log plot shows percent BM and spleen CD34$^-$KSL cells lacking BrdU uptake. BM data significantly differed from spleen data ($p < 0.0001$). The mean turnover times were approximately 13 days or 25 days for spleen or BM CD34$^-$KSL cells, respectively. The 50% turnover times were approximately 9 or 17 days for spleen or BM CD34$^-$KSL cells, respectively.

[27]. In this study, the kinetics of BrdU uptake differed between spleen and BM HSCs. We infer that the kinetics of BrdU uptake also should differ between spleen and PB HSCs, supporting our conclusion that most spleen HSCs do not readily exchange places with circulating HSCs.

Osteoblasts have been proposed as a constituent of the BM niche [7–9], and endochondral ossification is reportedly required for niche formation [28]. Vascular endothelial cells are another good candidate for niche constituent cells [10]. The spleen niche is supposedly composed of vascular endothelial cells but not of osteoblasts. Difference in cell-cycle coordination for large numbers of HSCs may result from distinct niche components in each organ. If this is the case, osteogenesis-related elements should play a role in prolonging quiescence in BM HSCs and not in spleen HSCs. Of importance, however, is that HSC quiescence takes place regardless of the absence of osteoblasts. If niche itself is similar between BM and spleen, to postulate a control center for widely distributed niches (in BM or spleen) may be necessary. Such a center would signal to BM and spleen niches in different manners.

We do not know how and to what extent spleen HSCs contribute to hematopoiesis under physiological conditions. Spleen HSCs seem not to differentiate in the same way as BM HSCs. Differentiation pathways from spleen HSCs possibly differ from those of BM HSCs. Because differentiation pathways for BM HSCs are still debated [29,30], it is interesting to compare road maps of differentiation between BM and spleen HSCs. Rapid erythropoiesis takes place in mouse spleen when acute hemolytic anemia is induced by phenylhydrazine [31]. The spleen may serve as a reservoir of HSCs for relatively immediate use. In this regard, a short

G_0 time may work as an advantage for spleen HSCs so that they can give rise to progeny with little delay.

Acknowledgments

We are grateful to Dr. A. S. Knisely for critical review of the manuscript. This work was supported by grants from the Ministry of Education, Culture, Sport, Science, and Technology, Japan.

Conflict of interest disclosure

No financial interest/relationships with financial interest relating to the topic of this article have been declared.

References

1. Metcalf D, Moore MAS. Haemopoietic cells. Amsterdam: North-Holland Publishing Co; 1971.
2. Christensen JL, Wright DE, Wagers AJ, Weissman IL. Circulation and chemotaxis of fetal hematopoietic stem cells. PLoS Biol. 2004;2:E75.
3. Gekas C, Dieterlen-Lievre F, Orkin SH, Mikkola HK. The placenta is a niche for hematopoietic stem cells. Dev Cell. 2005;8:365–375.
4. Ottersbach K, Dzierzak E. The murine placenta contains hematopoietic stem cells within the vascular labyrinth region. Dev Cell. 2005; 8:377–387.
5. Schofield R. The relationship between the spleen colony-forming cell and the haemopoietic stem cell. Blood Cells. 1978;4:7–25.
6. Kiel MJ, Morrison SJ. Uncertainty in the niches that maintain haematopoietic stem cells. Nat Rev Immunol. 2008;8:290–301.
7. Zhang J, Niu C, Ye L, et al. Identification of the haematopoietic stem cell niche and control of the niche size. Nature. 2003;425:836–841.
8. Calvi LM, Adams GB, Weibrecht KW, et al. Osteoblastic cells regulate the haematopoietic stem cell niche. Nature. 2003;425:841–846.
9. Arai F, Hirao A, Ohmura M, et al. Tie2/angiopoietin-1 signaling regulates hematopoietic stem cell quiescence in the bone marrow niche. Cell. 2004;118:149–161.
10. Kiel MJ, Yilmaz OH, Iwashita T, Yilmaz OH, Terhorst C, Morrison SJ. SLAM family receptors distinguish hematopoietic stem and progenitor cells and reveal endothelial niches for stem cells. Cell. 2005;121:1109–1121.
11. Sugiyama T, Kohara H, Noda M, Nagasawa T. Maintenance of the hematopoietic stem cell pool by CXCL12-CXCR4 chemokine signaling in bone marrow stromal cell niches. Immunity. 2006;25: 977–988.
12. Sacchetti B, Funari A, Michienzi S, et al. Self-renewing osteoprogenitors in bone marrow sinusoids can organize a hematopoietic microenvironment. Cell. 2007;131:324–336.
13. Morikawa S, Mabuchi Y, Kubota Y, et al. Prospective identification, isolation, and systemic transplantation of multipotent mesenchymal stem cells in murine bone marrow. J Exp Med. 2009;206:2483–2496.
14. Mendez-Ferrer S, Michurina TV, Ferraro F, et al. Mesenchymal and haematopoietic stem cells form a unique bone marrow niche. Nature. 2010;466:829–834.
15. Harrison DE, Jordan CT, Zhong RK, Astle CM. Primitive hemopoietic stem cells: direct assay of most productive populations by competitive repopulation with simple binomial, correlation and covariance calculations. Exp Hematol. 1993;21:206–219.
16. Szilvassy SJ, Humphries RK, Lansdorp PM, Eaves AC, Eaves CJ. Quantitative assay for totipotent reconstituting hematopoietic stem cells by a competitive repopulation strategy. Proc Natl Acad Sci U S A. 1990;87:8736–8740.
17. Wright DE, Wagers AJ, Gulati AP, Johnson FL, Weissman IL. Physiological migration of hematopoietic stem and progenitor cells. Science. 2001;294:1933–1936.
18. Ema H, Morita Y, Yamazaki S, et al. Adult mouse hematopoietic stem cells: purification and single-cell assays. Nat Protoc. 2006;1:2979–2987.
19. Harrison DE, Zsebo KM, Astle CM. Splenic primitive hematopoietic stem cell (PHSC) activity is enhanced by steel factor because of PHSC proliferation. Blood. 1994;83:3146–3151.
20. Sudo K, Ema H, Morita Y, Nakauchi H. Age-associated characteristics of murine hematopoietic stem cells. J Exp Med. 2000;192:1273–1280.
21. Ema H, Sudo K, Seita J, et al. Quantification of self-renewal capacity in single hematopoietic stem cells from normal and Lnk-deficient mice. Dev Cell. 2005;8:907–914.
22. Osawa M, Hanada K, Hamada H, Nakauchi H. Long-term lymphohematopoietic reconstitution by a single CD34-low/negative hematopoietic stem cell. Science. 1996;273:242–245.
23. Takano H, Ema H, Sudo K, Nakauchi H. Asymmetric division and lineage commitment at the level of hematopoietic stem cells: inference from differentiation in daughter cell and granddaughter cell pairs. J Exp Med. 2004;199:295–302.
24. Yamazaki S, Iwama A, Takayanagi S, et al. Cytokine signals modulated via lipid rafts mimic niche signals and induce hibernation in hematopoietic stem cells. EMBO J. 2006;25:3515–3523.
25. Bradford GB, Williams B, Rossi R, Bertoncello I. Quiescence, cycling, and turnover in the primitive hematopoietic stem cell compartment. Exp Hematol. 1997;25:445–453.
26. Lajtha LG. Stem cell concepts. Differentiation. 1979;14:23–34.
27. Bhattacharya D, Czechowicz A, Ooi AG, Rossi DJ, Bryder D, Weissman IL. Niche recycling through division-independent egress of hematopoietic stem cells. J Exp Med. 2009;206:2837–2850.
28. Chan CK, Chen CC, Luppen CA, et al. Endochondral ossification is required for haematopoietic stem-cell niche formation. Nature. 2009; 457:490–494.
29. Adolfsson J, Mansson R, Buza-Vidas N, et al. Identification of Flt3+ lympho-myeloid stem cells lacking erythro-megakaryocytic potential a revised road map for adult blood lineage commitment. Cell. 2005; 121:295–306.
30. Arinobu Y, Mizuno S, Chong Y, et al. Reciprocal activation of GATA-1 and PU.1 marks initial specification of hematopoietic stem cells into myeloerythroid and myelolymphoid lineages. Cell Stem Cell. 2007;1: 416–427.
31. Vannucchi AM, Paoletti F, Linari S, et al. Identification and characterization of a bipotent (erythroid and megakaryocytic) cell precursor from the spleen of phenylhydrazine-treated mice. Blood. 2000;95: 2559–2568.
32. Ema H, Nakauchi H. Expansion of hematopoietic stem cells in the developing liver of a mouse embryo. Blood. 2000;95:2284–2288.

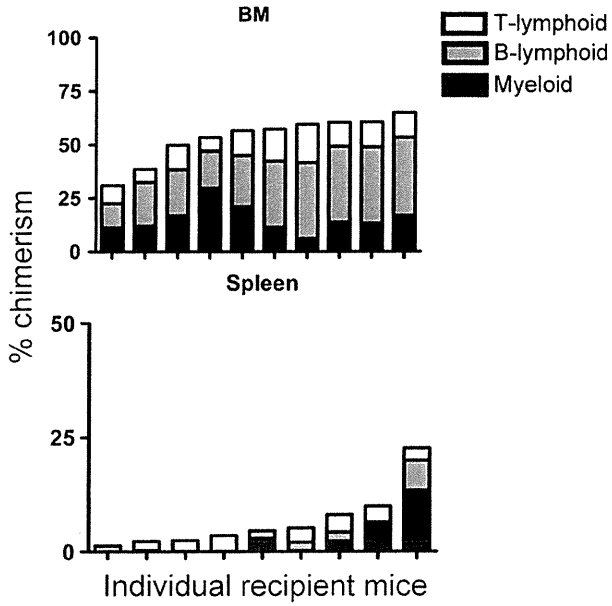

Supplementary Figure E1. Lineage reconstitution by whole BM or spleen cells Competitive repopulation was performed using whole BM or spleen cells. Recipient mice were analyzed 16 weeks after transplantation. Myeloid, B-lymphoid, and T-lymphoid lineage reconstitution are shown for individual recipient mice.

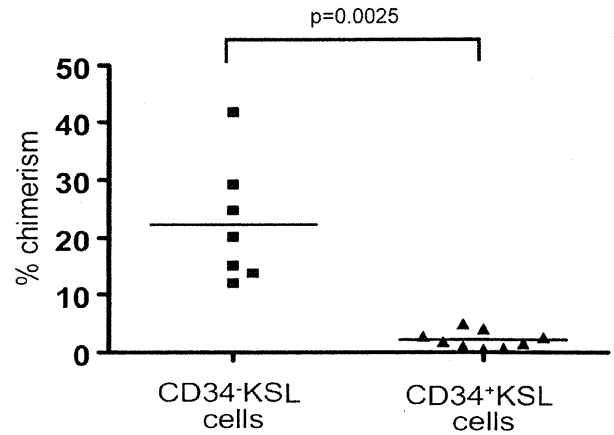

Supplementary Figure E2. CD34$^-$KSL cells are enriched in spleen HSC activity Individual lethally irradiated mice were transplanted with 100 CD34$^-$ or CD34$^+$KSL cells isolated from spleen along with 2×10^5 BM competitor cells. Recipient mice were analyzed 16 weeks after transplantation. Percent chimerism conferred by CD34$^-$ and CD34$^+$KSL cells was 22.3 ± 10.6 (mean ± SD, n = 7) or 2.2 ± 1.5 (n = 9), respectively. Unpaired *t*-testing (with Welch correction) showed a significant difference between the groups ($p = 0.0025$).

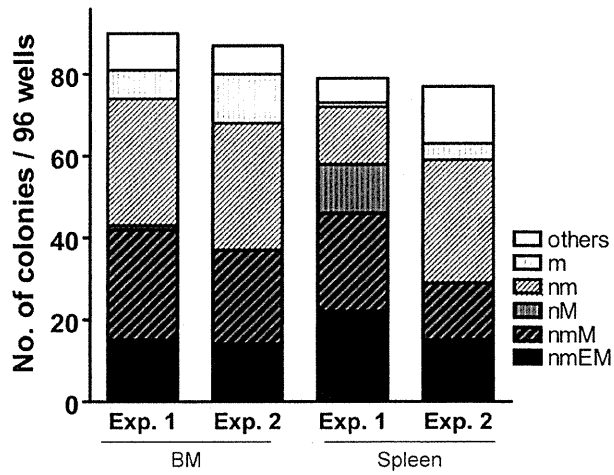

Supplementary Figure E3. Single-cell cultures with CD34$^-$KSL BM or spleen cells CD34$^-$KSL cells from BM or spleen were individually sorted into each well of a 96-well microtiter plate. Cells were cultured for 14 days in the presence of stem cell factor, thrombopoietin, interleukin-3, and erythropoietin. Cytocentrifugation was performed on each colony to permit light-microscopy morphological examination of colony-composing cells. Data from two individual experiments are shown. E = erythroblasts; m = macrophages; M = megakaryocytes; n = neutrophils.

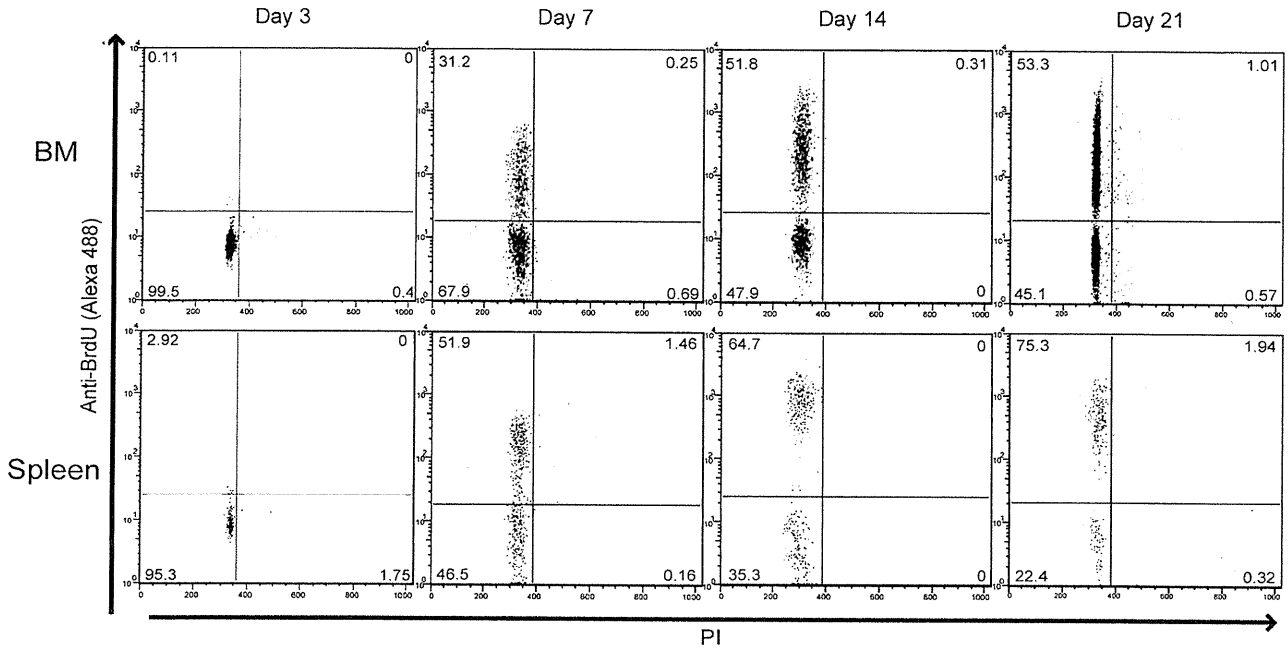

Supplementary Figure E4. Flow cytometric analysis of BrdU uptake by $CD34^{-}$KSL cells. Groups of 10 mice received BrdU in drinking water for 3, 7, 14, or 21 days. BM and spleen cells obtained from each group of mice were pooled. $CD34^{-}$KSL cells isolated from pooled BM or spleen cells were stained with anti-BrdU antibody, followed by propidium iodide (PI) staining. The upper and lower panels show BM and spleen cells, respectively. These data are graphically presented in Figure 5B.

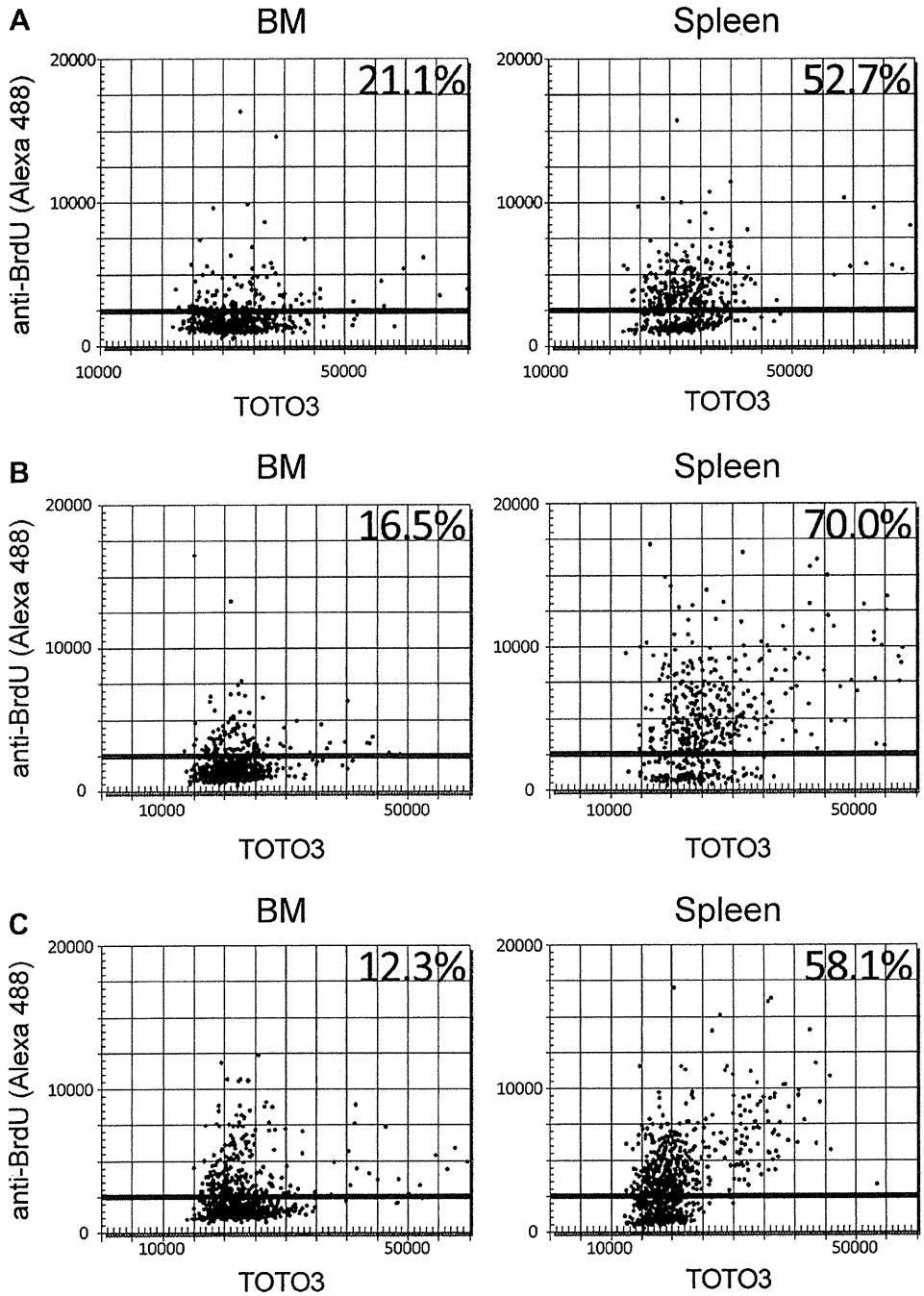

Supplementary Figure E5. Arrayscan analysis of BrdU uptake by $CD34^{-}KSL$ cells. Groups of 3 to 5 mice received BrdU in drinking water for 7 days; 1000 to 2000 BM and spleen CD34-KSL cells were isolated from each group and placed on glass slides. After staining with anti-BrdU antibody and TOTO3, 500 to 1000 cells were analyzed and data were collected with Arrayscan. (**A**) BM or spleen $CD34^{-}KSL$ cells from normal mice were analyzed. (**B**) Lethally irradiated mice (Ly5.2) were transplanted with 1×10^6 BM cells (Ly5.1). Mice were used for BrdU-uptake analysis 12 months after transplantation. BM or spleen $Ly5.1^{+}CD34^{-}KSL$ cells from reconstituted mice were analyzed. (**C**) Lethally irradiated mice (Ly5.2) were transplanted with 3×10^7 spleen cells (Ly5.1). Mice were used for BrdU-uptake analysis 12 months after transplantation. BM or spleen $Ly5.1^{+}CD34^{-}KSL$ cells from reconstituted mice were analyzed.

Published OnlineFirst on January 6, 2012; DOI:10.1158/1541-7786.MCR-11-0347

Molecular Cancer Research

Fibroblast Growth Factor-2 Is an Important Factor that Maintains Cellular Immaturity and Contributes to Aggressiveness of Osteosarcoma

Takatsune Shimizu, Tomoki Ishikawa, Sayaka Iwai, et al.

Mol Cancer Res Published OnlineFirst January 6, 2012.

Published OnlineFirst on January 6, 2012; DOI:10.1158/1541-7786.MCR-11-0347

Molecular Cancer Research

Signaling and Regulation

Fibroblast Growth Factor-2 Is an Important Factor that Maintains Cellular Immaturity and Contributes to Aggressiveness of Osteosarcoma

Takatsune Shimizu[1,7], Tomoki Ishikawa[1,6], Sayaka Iwai[1,3], Arisa Ueki[1], Eiji Sugihara[1,7], Nobuyuki Onishi[1], Shinji Kuninaka[1], Takeshi Miyamoto[3], Yoshiaki Toyama[3], Hiroshi Ijiri[8], Hajime Mori[8], Yumi Matsuzaki[4], Tomonori Yaguchi[2], Hiroshi Nishio[2], Yutaka Kawakami[2], Yasuo Ikeda[5], and Hideyuki Saya[1,7]

Abstract

Osteosarcoma is the most frequent, nonhematopoietic, primary malignant tumor of bone. Histopathologically, osteosarcoma is characterized by complex mixtures of different cell types with bone formation. The role of environmental factors in the formation of such a complicated tissue structure as osteosarcoma remains to be elucidated. Here, a newly established murine osteosarcoma model was used to clarify the roles of environmental factors such as fibroblast growth factor-2 (Fgf2) or leukemia-inhibitory factor (Lif) in the maintenance of osteosarcoma cells in an immature state. These factors were highly expressed in tumor environmental stromal cells, rather than in osteosarcoma cells, and they potently suppressed osteogenic differentiation of osteosarcoma cells *in vitro* and *in vivo*. Further investigation revealed that the hyperactivation of extracellular signal–regulated kinase (Erk)1/2 induced by these factors affected in the process of osteosarcoma differentiation. In addition, Fgf2 enhanced both proliferation and migratory activity of osteosarcoma cells and modulated the sensitivity of cells to an anticancer drug. The results of the present study suggest that the histology of osteosarcoma tumors which consist of immature tumor cells and pathologic bone formations could be generated dependent on the distribution of such environmental factors. The combined blockade of the signaling pathways of several growth factors, including Fgf2, might be useful in controlling the aggressiveness of osteosarcoma. *Mol Cancer Res; 1–15. ©2012 AACR.*

Introduction

Osteosarcoma is the most frequent, nonhematopoietic, primary malignant tumor of bone. Osteosarcoma is characterized by aggressive local growth and systemic hematogenous dissemination, which together confer a generally poor prognosis (1, 2). The identification of osteoid (dense, amorphous intercellular material of immature bone) production by tumor cells was one of the critical findings for the diagnosis of osteosarcoma (3). Histopathologically, osteosarcoma is characterized by complex mixtures of different cell types with bone formation (3). Previous reports have suggested that the response to therapies and prognosis of malignant tumors are greatly influenced by the differentiation state of tumor cells and by histologic subtypes (4, 5). Moreover, the extracellular matrix produced by tumor cells protects tumors from apoptosis induced by anticancer agents (6, 7). Considering these points, the difficulty of osteosarcoma treatment might be related to the tissue heterogeneity within osteosarcoma tumors.

Malignant tumors are composed of transformed neoplastic cells and tumor stroma containing a variety of extracellular matrix components and cell types such as fibroblasts, endothelial cells, and hematopoietic cells (8, 9). Accumulated evidence has clarified that cytokines, chemokines, and growth factors released from tumor stroma play critical roles in the promotion of tumor progression (10, 11). However, it remains to be elucidated how osteosarcoma microenvironments could contribute to osteosarcoma progression or the formation of such a complicated histopathology as the mixture of immature cells and osteogenic differentiation areas. Clarification of environmental effects may provide important clues towards the development of novel therapeutic approaches as well as the elucidation of osteosarcoma pathogenesis.

Previously, we developed a novel osteosarcoma mouse model by overexpressing c-MYC in bone marrow stromal cells (BMSC) derived from mice with a homozygous deletion of the Ink4a/Arf locus (12). We isolated highly tumorigenic cells (designated AX cells) from the BMSCs using

Authors' Affiliations: Divisions of [1]Gene Regulation and [2]Cellular Signaling, Institute for Advanced Medical Research, Departments of [3]Orthopedic Surgery, [4]Physiology, and [5]Internal Medicine, Keio University School of Medicine, Keio University; [6]Kasai R&D Center, Daiichi Sankyo Co. Ltd.; [7]CREST, Japan Science and Technology Agency, Tokyo; and [8]Insect Biomedical Research Center, Kyoto Institute of Technology, Kyoto, Japan

Note: Supplementary data for this article are available at Molecular Cancer Research Online (http://mcr.aacrjournals.org/).

Corresponding Author: Hideyuki Saya, Division of Gene Regulation, Institute for Advanced Medical Research, Keio University School of Medicine, Tokyo 160-8582, Japan. Phone: 81-3-5363-3981; Fax: 81-3-5363-3982; E-mail: hsaya@a5.keio.jp

doi: 10.1158/1541-7786.MCR-11-0347

Published OnlineFirst on January 6, 2012; DOI:10.1158/1541-7786.MCR-11-0347

single cell cloning. Inoculation of AX cells into syngeneic C57BL/6 mice results in the development of lethal osteosarcoma with metastatic lesions in various organs, including lung, which mimics human osteoblastic osteosarcoma. Although AX cells are maintained in an immature state *in vitro*, they generate mature bone and tumors that contain structures with heterogeneous differentiation patterns *in vivo*.

In the present study, fibroblast growth factor-2 (Fgf2), leukemia-inhibitory factor (Lif), and insulin-like growth factor 1 (Igf1) were focused on as the factors highly expressed in the tumor environment rather than in osteosarcoma cells. Further investigation revealed that the hyperphosphorylation of extracellular signal–regulated kinase (Erk)1/2 in AX cells induced by Fgf2 or Lif potently suppressed osteogenic differentiation. Erk1/2 hyperactivation was detected at the immature areas of tumors, suggesting that it plays key roles in maintaining immaturity in osteosarcoma cells *in vivo*. In addition, Fgf2 afforded a growth advantage and the enhancement of cellular motility, as well as resistance to Adriamycin, to AX cells, indicating the contribution of Fgf2 to tumor progression and refractoriness to treatment.

Our results suggest that the complex histology of osteosarcoma is generated, depending on the distribution of environmental growth factors.

Materials and Methods

Cell culture

Mouse osteosarcoma AX cells were established as previously described (12) and were cultured in Iscove's Modified Dulbecco's Medium (IMDM; Invitrogen) supplemented with 20% FBS. Human osteosarcoma cell lines (SAOS2, U2OS, and SJSA1) were purchased from American Type Culture Collection (ATCC) and cultured in Dulbecco's Modified Eagle's Medium (DMEM) high glucose (Invitrogen) supplemented with 10% FBS.

Differentiation assays

For the induction of osteogenesis, cells were spread on 8-well chamber culture slides (BD Biosciences) with 80% confluency. The next day, the culture medium was changed to IMDM supplemented with 10% FBS, 20 mmol/L β-glycerophosphate (Sigma-Aldrich), 50 ng/mL thyroxine (Sigma-Aldrich), 1 nmol/L dexamethasone (Sigma-Aldrich), and 0.5 μmol/L ascorbate-2-phosphate (Sigma-Aldrich). This culture medium was designated osteogenic medium (OG medium) in the article. In some assays, human FGF2 (Peprotech), mouse Lif (ESGRO; 1,000 U = 1 ng; Millipore), mouse Fgf1 (R&D), or mouse Igf1 (R&D) was added to osteogenic medium at the indicated concentrations. For the inhibition of Fgf receptor (Fgfr) or Mek, cells were cultured in osteogenic medium supplemented with Fgf2 or Lif plus each inhibitor, PD173074 (Sigma-Aldrich), and SU5402 (Calbiochem) for Fgfr inhibition, or U0216 (Calbiochem) and PD98059 (Cayman Chemical) for Mek inhibition, 1 hour after the pretreatment of each inhibitor alone in osteogenic medium. The medium was changed every third day. Cells were fixed in 4% paraformaldehyde for 20 minutes at room temperature and then stained with Alizarin Red S (Sigma-Aldrich) at pH 4.3.

Flow cytometry

Subcutaneous AX-derived osteosarcoma tumors were excised from euthanized mice. They were minced and incubated in IMDM supplemented with 2% FBS, 50 U/mL collagenase I (Worthington), 100 U/mL collagenase IV (Worthington), 2.5 U/mL collagenase XIV (Sigma-Aldrich), and 20 U/mL DNaseI (Sigma-Aldrich) for 2 hours at 37°C. The cell suspension was washed with PBS and filtered through a 40-μm cell strainer (BD Biosciences), and single-cell suspensions were prepared. For blocking of Fc receptors, the suspensions were treated with anti-mouse CD16/CD32 antibody (1:100; e-Bioscience) for 15 minutes on ice. Then they were incubated with phycoerythrin (PE)-conjugated antibodies to CD45, F4/80, and APC-conjugated Sca1 antibody (e-Bioscience). The labeled cells were analyzed with FACSCalibur and Cell Quest software (BD Biosciences). At least 10,000 live cells were examined. GFP-positive, GFP-negative-plus-F4/80-positive, or GFP/CD45-negative-plus-Sca1-positive fractions were sorted by Vantage SE flow cytometer (BD Biosciences).

Cell proliferation assay

Cells were transferred to 96-well tissue culture plates and cultured in IMDM supplemented with 10% FBS, Adriamycin, and/or the indicated growth factors. Cell proliferation was measured with the use of a CellTiter-Glo cell proliferation assay kit (Promega). All assays were conducted in triplicate.

RNA interference

Knockdown of Fgfr1 and Fgfr2 was carried out using premade Stealth select siRNA (FGFR1MSS204294, 204295, 274341, FGFR2MSS204296, 204298) purchased from Invitrogen. The control siRNA for firefly luciferase (GL2); 5′-CGUACGCGGAAUACUUCGATT-3′ was purchased from Japan Bio Services. A total of 50 nmol/L of each siRNA was transfected to AX cells according to the manufacturer's instruction and continuously treated during differentiation assays.

Immunoblot analysis

Cells were lysed with Laemmli sample buffer (BioRad) supplemented with β-mercaptoethanol (Sigma-Aldrich), and immunoblot analyses were conducted according to standard procedures with primary antibodies to phospho-Erk1/2 (Cell Signaling Technologies), Erk1/2 (Cell Signaling Technologies), phospho-Akt (Cell Signaling Technologies), Akt (Cell Signaling Technologies), Fgfr1 (Epitomics), Fgfr2 (Santa Cruz Biotechnology), and α-Tubulin (Sigma-Aldrich). In some assays, human FGF2, mouse Fgf1, mouse Lif, or mouse Igf1 was added and incubated for the indicated times. For the inhibition of Fgfr or Mek, cells were cultured with each factor and each inhibitor 1 hour after pretreatment with each inhibitor alone.

Published OnlineFirst on January 6, 2012; DOI:10.1158/1541-7786.MCR-11-0347

Tumor xenograft model

All animal care and procedures were conducted in accordance with the guidelines of Keio University (Tokyo, Japan). All mice were purchased from SLC. For xenograft experiments, AX cells were suspended in PBS and then injected subcutaneously into syngeneic 8-week-old female C57BL/6 mice. For intrabone marrow injection, AX cells were injected into a tiny hole made with a 23G needle at the intercondylar fossa of a femur. To overexpress Fgf2 and Lif in tumors *in vivo*, 2 million AX cells were mixed with Fgf2 polyhedra (125 ng of Fgf2 per an injection; refs. 13, 14) or Lif polyhedra (25 ng of Lif per an injection; ref. 15) suspended in PBS containing 50 ng/mL Fgf2 or 1,000 U/mL Lif, respectively and subcutaneously injected. Two weeks later, mice were euthanized and tumors were subjected to immunohistochemistry. To investigate the effect of a combined treatment of PD173074 (Sigma-Aldrich) and Adriamycin, 2 million AX cells were subcutaneously inoculated (day 0). Eleven days later, PD173074 was administered intraperitoneally at 10 mg/kg every other day 6 times in total. Eight mg/kg of Adriamycin was intravenously injected on day 14. On day 22, all mice were euthanized and tumors were subjected to analyses.

Gene expression profiling

The gene expression profiling of AX cells sorted from tumors was carried out using the 3D-Gene Chip (Toray) as previously described (12).

Real-time reverse transcriptase PCR analysis

Total RNA was extracted with RNeasy Mini Spin columns (Qiagen) and was subjected to reverse transcriptase by the Prime Script RT-PCR kit (Takara).

Real-time reverse transcriptase (RT)-PCR analysis was conducted using SYBR Premix Ex TaqII and Thermal Cycler Dice (Takara). Data are represented as means ± SD from 3 independent experiments. The sequences of the primers used in this study are shown in Supplementary Table S1.

Immunohistochemistry

Immunohistochemical analysis was conducted using standard methods. Deparaffinized sections were stained with antibodies to GFP, Fgf2, Lif, Runx2, Fgfr2 (Santa Cruz Biotechnology), Igf1 (R&D), Fgfr1 (Epitomics), Fgfr3 (Assay Biotechnology), CD31 (Abcam), or phospho-Erk1/2. For anti-mouse primary antibodies, the pretreatment was carried out by MOM kit (Vector Laboratories) to avoid nonspecific staining. Immune complexes were detected with the use of Histofine (Nichirei Bioscience) and Simple Stain kit (Nichirei Bioscience). For immunofluorescence staining, deparaffinized sections were stained with rabbit polyclonal anti-GFP (Santa Cruz Biotechnology) or mouse monoclonal anti-GFP antibody (MBL) followed by Alexa488-conjugated anti-rabbit IgG or anti-mouse IgG secondary antibody (Invitrogen), respectively, anti-F4/80 antibody followed by Alexa555-conjugated anti-rat IgG secondary antibody (Invitrogen), anti-Fgf2 antibody followed by Alexa555-conjugated anti-rabbit IgG secondary antibody (Invitrogen), or an APC-conjugated Sca1 antibody (e-Bioscience). TOTO3 (Invitrogen) was used for nuclear staining. Prepared samples were observed with confocal microscopy (LSM510; Zeiss) and analyzed with an LSM image browser (Zeiss).

Quantitative protein analysis of Fgf2, Lif, and Vegfa

To acquire tumor homogenate, tumors and adjacent host tissues were suspended with an equivalent volume of cell lysis buffer (MBL) and mashed with Biomasher (Nippi). The concentration of Fgf2, Lif, and Vegfa in the lysates was quantified by Bio-Plex Pro Mouse Cytokine 9-plex Assay G2 (BioRad) according to the manufacturer's instruction.

Migration assay

Transwell migration assays were conducted with Transwell membrane filter inserts with 8-μm pores (BD Biosciences) in 24-well tissue culture plates. AX cells (50,000 cells) were replated onto the upper chamber in 500 μL of serum-free IMDM supplemented with 50 ng/mL of Fgf2, 2,000 U/mL of Lif, 10 ng/mL of Igf1, and the mixture of each factor. The chamber was placed in 750 μL of IMDM supplemented with 1% FBS with the same concentration of each factor as the upper chamber. After 4 hours of incubation at 37°C in 5% CO_2, cells on the upper surface of the filter were removed by wiping with a moist cotton swab. The cells migrated through the filter and adhered to its lower surface, where they were fixed, stained by a Diff-Quick kit (Sysmex) and counted under the microscope. Each assay was conducted in triplicate.

Results

Immature osteosarcoma cells were located in the periphery of tumors

We recently developed a mouse osteosarcoma model (12). Highly tumorigenic AX cells, which overexpressed enhanced GFP (EGFP) in addition to c-MYC, were isolated from the BMSCs by single cell cloning. Upon subcutaneous injection into syngeneic C57BL/6 mice, AX cells developed lethal metastatic osteosarcoma (12). Tumors consisted of both immature cells and the region of mature bone formation (Fig. 1A). Notably, immature cells were accumulated in the peripheral part of the tumor, whereas bone formations were apparent inside the tumor (Fig. 1A). We speculated that the differentiation state of tumor cells was affected by the components of the tumor microenvironment, resulting in the formation of histologic heterogeneity of osteosarcoma.

First, we tried to identify the cellular components of osteosarcoma. Single-cell suspensions from AX-derived osteosarcoma tumors were stained with PE-conjugated anti-CD45 antibody and analyzed by flow cytometry (Fig. 1B). Three fractions were identified in osteosarcoma tumors: GFP-positive AX cells, CD45-positive hematopoietic cells, and the remaining fraction without GFP or CD45 expression (Fig. 1B). Because the majority of CD45-positive hematopoietic cells also expressed a mature macrophage marker, F4/80 (Fig. 1C), F4/80-positive cells were sorted and used for further analyses (Fig. 1D). These macrophages highly express genes related to the M2 phenotype such as Mmp1, Tnfα, Il10, and Arginase, suggesting that they seem to be tumor-associated

Published OnlineFirst on January 6, 2012; DOI:10.1158/1541-7786.MCR-11-0347

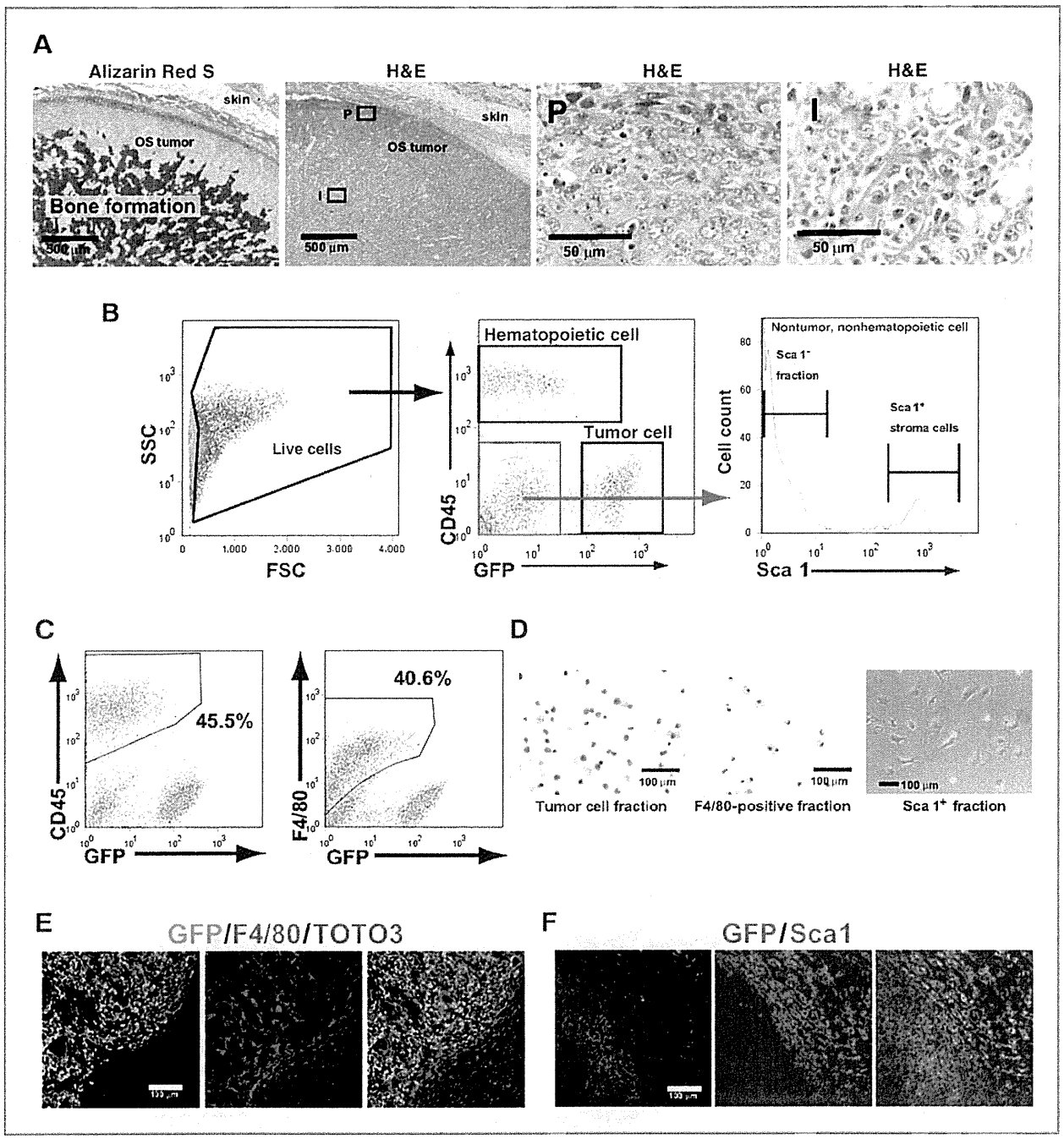

Figure 1. Histology of mouse osteosarcoma. A, Alizarin Red S (left) and hematoxylin–eosin (H&E) staining of mouse osteosarcoma (OS) serial sections. Boxed regions are shown at a higher magnification in the right. P, immature cells were enriched at the peripheral part of osteosarcoma; I, osteogenesis with marked osteoid production was apparent mainly inside the tumor. B, osteosarcoma tumors were dissected and minced into single-cell suspension and analyzed for GFP, CD45, and Sca1 positivity by flow cytometry. C, CD45- and F4/80-positive hematopoietic cells in osteosarcoma were analyzed by flow cytometry. D, morphology of sorted cells. GFP-positive osteosarcoma cells and F4/80-positive hematopoietic cells were cytospun and stained with May–Giemsa. The primary culture of Sca1-positive fibroblasts is also shown. E, confocal microscopic analysis of GFP- and F4/80-expressing cells in an osteosarcoma tumor. TOTO3 was used for nuclear staining. F, immunofluorescence analysis of GFP and Sca1 expression in an osteosarcoma tumor. Sca1-positive cells were located around the GFP-positive tumor cells. SSC, side scatter; FSC, forward scatter.

Published OnlineFirst on January 6, 2012; DOI:10.1158/1541-7786.MCR-11-0347

macrophages (16, 17 and data not shown). Immunofluorescence analysis revealed that macrophages gathered around and inside the osteosarcoma tumors (Fig. 1E). GFP-positive AX cells were small and exhibited a high nuclear/cytosolic ratio (Fig. 1D). The third fraction, without GFP or CD45 expression, contained a heterogeneous population of cells composed mainly of fibroblastic stromal cells, as well as debris. To enrich the live fibroblasts, Stem cell antigen 1 (Sca1) was used, which was suggested to be expressed in the multipotent dermal fibroblasts (18, 19). Live fibroblasts were successfully enriched with an APC-conjugated Sca-1 antibody and these were located around the tumors (Fig. 1B, D, and F). Collectively, AX-derived tumors were consisted of fibroblasts and macrophages as well as osteosarcoma cells, and the interfacial regions of tumors were composed of immature tumor cells.

Environmental factors promote osteosarcoma tumor cell proliferation and suppress osteogenesis

Detailed observations of mouse subcutaneous osteosarcoma indicated that tumor cells that did not directly contact surrounding nontumor cells also exhibited immature states (Fig. 1A). Thus, to elucidate the environmental effects on the generation of histologic heterogeneity of osteosarcoma, we focused on the soluble factors, rather than the molecules involved in direct cell to cell contact. The gene expression profile of tumor cells sorted from AX-derived osteosarcoma tumors was used for the initial screening. Given that we intended to exclude the effects of factors released from tumor cells, we focused on secreted soluble factors whose gene expression levels were extremely low in tumor cells (Supplementary Table S2). Among these factors the mRNA levels of *Fgf1*, *Fgf2*, *Igf1*, *Igf2*, *Lif*, and hepatocyte growth factor (*Hgf*) were evaluated in tumor cells and sorted environmental components by real-time RT-PCR analysis. *Fgf1*, *Fgf2*, *Lif*, and *Igf1* exhibited markedly higher expression in macrophages or fibroblasts than tumor cells (Fig. 2A and data not shown) and they were subjected to further analyses. These factors afforded a growth advantage to AX cells *in vitro* (Fig. 2B). Fgf1, Fgf2, and Lif significantly enhanced cell growth and Fgf2 exhibited the most potent effect. Igf1 also showed a slight tendency to promote cell growth, albeit without statistical significance. Importantly, the mixture of Fgf2, Lif, and Igf1 possessed additive effect compared with treatment of each factor alone.

Next, the effects of these factors on the osteogenic ability of AX cells were evaluated. After 7 days of culture in the osteogenic medium, AX cells produced mineralized

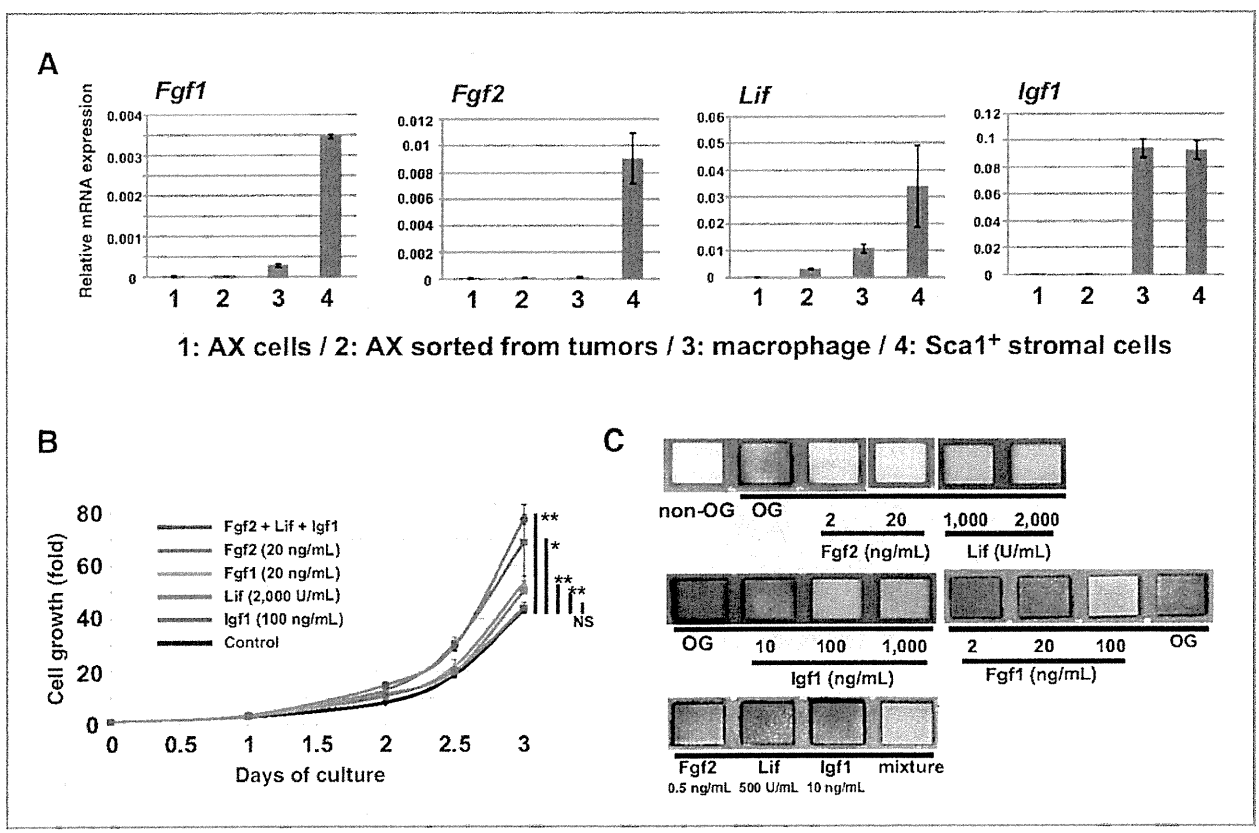

Figure 2. Environmental growth factors support osteosarcoma cell growth and suppress osteogenesis. A, real-time RT-PCR analyses of *Fgf1*, *Fgf2*, *Lif*, and *Igf1* genes in AX cells and sorted cells from osteosarcoma tumors. Results are shown as the ratio of the abundance of each mRNA to that of glyceraldehyde-3-phosphate dehydrogenase (*Gapdh*; $n = 3$). B, cell proliferation was analyzed with or without the indicated factors. Data are shown as the ratio of the measurement of each time point to that of day 0 and represented as means ± SD from 3 independent experiments. *, $P < 0.05$; **, $P < 0.005$; NS, not significant (the Student *t* test). C, osteogenesis was evaluated by Alizarin Red S staining of cells in osteogenic medium with or without the indicated factors for 7 days. OG, osteogenic culture condition.

Published OnlineFirst on January 6, 2012; DOI:10.1158/1541-7786.MCR-11-0347

materials and exhibited osteogenesis, as evaluated by the intracellular calcium deposition with Alizarin Red S staining (Fig. 2C), whereas under the control nonosteogenic medium AX cells did not exhibit osteogenesis. The supplementation of Fgf2 or Lif into the osteogenic medium potently suppressed these osteogenic processes resulting in negative staining for Alizarin Red S (Fig. 2C). Fgf1 also exhibited suppressive effect on osteogenesis, although the higher dose was required than Fgf2. The effect of Igf1 was modest and osteogenic ability in AX cells was still maintained at 1 μg/mL of Igf1. Importantly, these factors exhibited an additive effect and the combination of each factor at an insufficient dose to inhibit osteogenesis could potently block the differentiation process (Fig. 2C). These findings indicated that several environmental factors, such as Fgf1, Fgf2, or Lif may contribute to both the suppression of osteogenic differentiation and the enhancement of proliferation in osteosarcoma cells.

The treatment of Fgf2 hyperactivated Erk1/2 in AX cells

To investigate the molecular mechanisms that affect osteogenic ability, the downstream signaling pathways of receptors of Fgf, Lif, and Igf1 were analyzed by Western blotting. Previous reports indicated that the Map/Erk kinase (Mek)-Erk1/2 pathway or phosphoinositide 3-kinase (PI3K)-Akt pathways were activated by treatment with these factors (20–22). Although the phosphorylation level of Erk1/2 in AX cells increased after treatment with Fgf1, Fgf2, Lif, and Igf1, Fgf2 was the most potent activator among them (Fig. 3A and B; Supplementary Fig. S1A). The Erk1/2 phosphorylation was enhanced 20 minutes after Fgf2 treatment, and continued more than 6 hours, whereas in the cases of Fgf1, Lif, or Igf1 treatment, this activation returned to the same level as the normal culture condition in 6 hours (Fig. 3C; Supplementary Fig. S1A). Moreover, the phosphorylation level in AX cells treated with Igf1 was weaker compared with those treated with other factors. Stat3 was also phosphorylated by Lif treatment, as previously reported (21). Akt was constitutively phosphorylated even under normal culture conditions. Its phosphorylation was markedly enhanced by treatment with Igf1 (Fig. 3D). In contrast, treatment with Fgf1, Fgf2, and Lif scarcely affected the phosphorylation status of Akt in AX cells (Fig. 3D; Supplementary Fig. S1B and data not shown). Moreover, Fgf2 supplemented with Fgfr inhibitors did not change Akt activation (Supplementary Fig. S1C). These results indicated that Fgf1, Fgf2, and Lif potently induced the phosphorylation of Erk1/2 without hyperactivating Akt, whereas Igf1 was mainly involved in the activation of the PI3K-Akt pathway in AX cells.

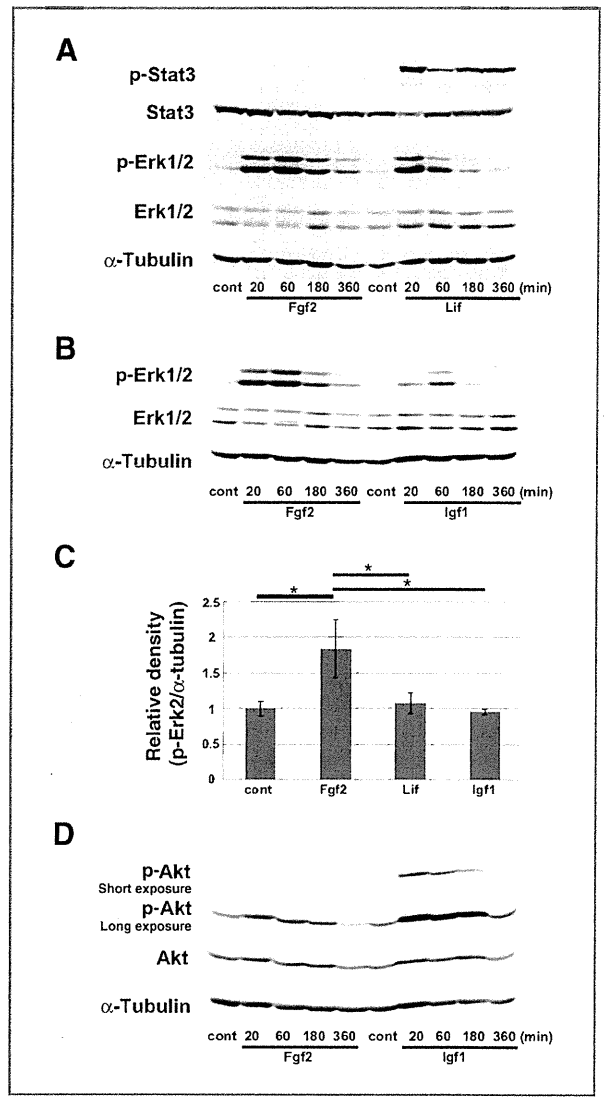

Figure 3. Fgf and Lif potently activated Erk1/2 in AX cells. A, Western blot analysis of phospho-Stat3, Stat3, phospho-Erk1/2, and Erk1/2 in AX cells treated with Fgf2 (20 ng/mL) and Lif (2,000 U/mL) for the indicated times. α-Tubulin was used as a loading control. B, phospho-Erk1/2 and Erk1/2 were assessed by immunoblotting. AX cells were treated with Fgf2 (20 ng/mL) or Igf1 (100 ng/mL) for the indicated times. α-Tubulin was used as a loading control. C, quantification of the phosphorylation level of Erk2 in AX cells treated with indicated factors for 6 hours. Results are shown by the ratio of the density of phospho-Erk2 (p-Erk2) to that of α-tubulin ($n = 3$). *, $P < 0.05$ (the Student t test). D, Western blot analysis of phospho-Akt and Akt in AX cells treated with Fgf2 (20 ng/mL) or Igf1 (100 ng/mL) for the indicated times. For Akt phosphorylation, photographs with both short- and long-time exposure are shown. α-Tubulin was used as a loading control.

Fgf2 reversibly inhibited the mRNA expression of osteogenic genes in AX cells

Given that Fgf2 enhanced cell growth and potently suppressed osteogenesis of AX cells *in vitro* (Fig. 2), its function was further assessed in osteosarcoma tissues. Immunofluorescence analyses revealed that Fgf2 was distributed mainly in the surrounding tissues and interfacial regions between tumor and stromal cells (Fig. 4A). Consistent with the gene expression patterns (Fig. 2A), Lif and Igf1 were also enriched in the surrounding tissues rather than inside the tumors (Supplementary Fig. S2A and S2B).

We also carried out intrabone marrow injections of AX cells to generate orthotopic osteosarcoma model

Published OnlineFirst on January 6, 2012; DOI:10.1158/1541-7786.MCR-11-0347

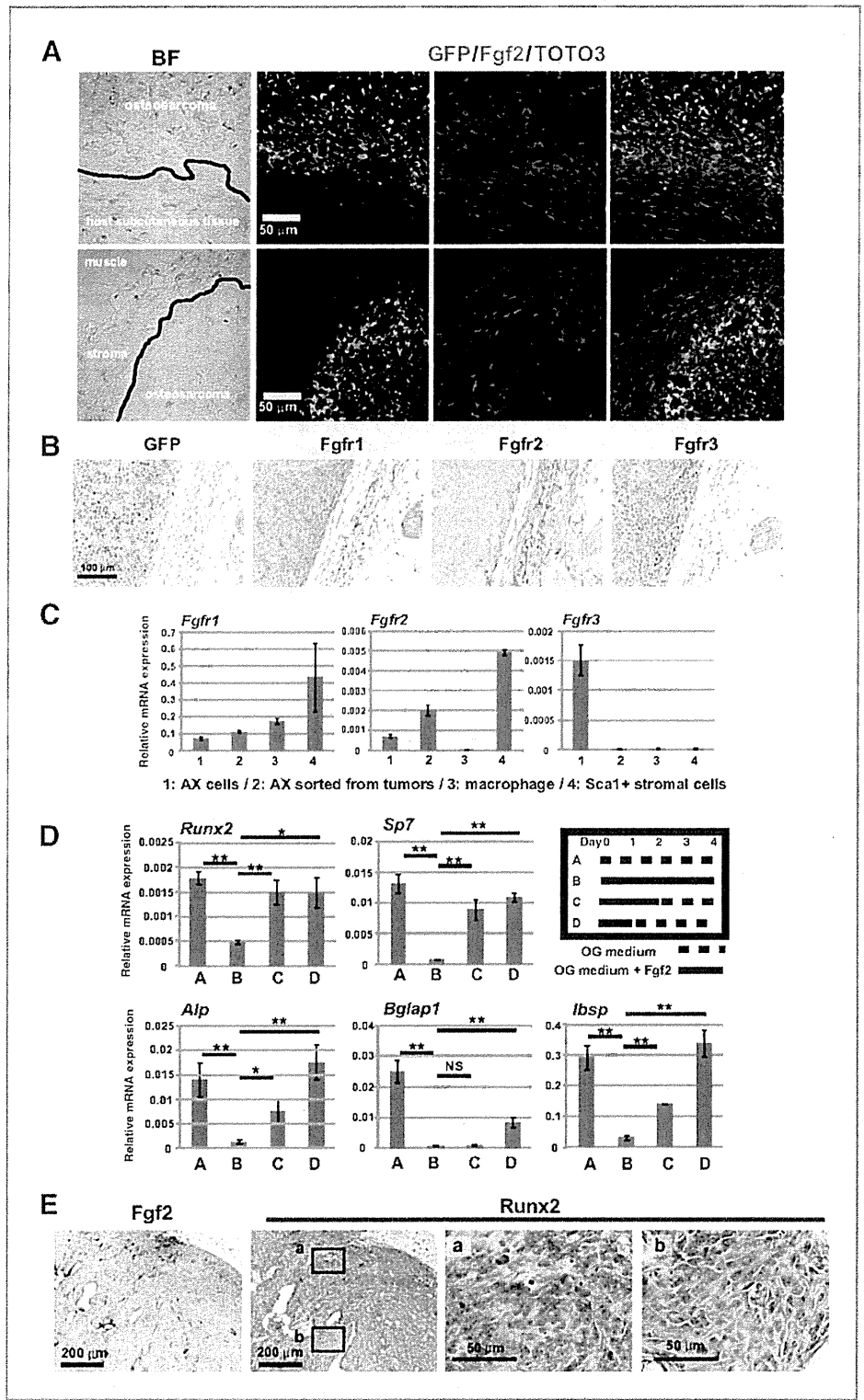

Figure 4. Fgf2 reversibly suppressed osteogenesis in AX cells. A, Fgf2 localization in osteosarcoma tumors was assessed by immunofluorescence analysis. Tumor cells were identified by GFP staining. TOTO3 was used for nuclear staining. BF, bright field. B, immunohistochemistry of serial sections of an AX-derived osteosarcoma tumor for GFP, Fgfr1, Fgfr2, and Fgfr3. C, real-time RT-PCR analysis of *Fgfr* genes in the indicated cells. Results are shown as the ratio of the abundance of each mRNA to that of *Gapdh*. ($n = 3$). D, AX cells were cultured in osteogenic (OG) medium supplemented with Fgf2 (20 ng/mL) according to the indicated schedule, and the expression of osteogenic genes was assessed by real-time RT-PCR analysis. Results are shown as the ratio of the abundance of each mRNA to that of *Gapdh*. ($n = 3$). *, $P < 0.05$; **, $P < 0.005$; NS, not significant (the Student *t* test). E, immunohistochemistry of serial sections of an AX-derived osteosarcoma tumor for Fgf2 and Runx2. Boxed regions are shown at a higher magnification in the right.

(Supplementary Fig. S2C). The intrabone tumor also showed bone differentiation accompanied by osteoid formations inside the tumors, and Fgf2 or Lif was stained in the surrounding regions of tumor cells. These factors appeared to be abundantly present inside normal bone marrow, suggesting that Fgf2 and Lif also modulate osteogenic differentiation of osteosarcoma cells in a bone microenvironment where human osteosarcoma tumors usually originate.

Published OnlineFirst on January 6, 2012; DOI:10.1158/1541-7786.MCR-11-0347

Quantitative protein analysis of Fgf2 and Lif revealed that the concentration from subcutaneous tumor homogenate was 668.1 ± 182.6 pg/mL ($n = 3$) and 39.12 ± 9.87 pg/ml ($n = 3$), respectively. Although these concentrations were lower than those we used in the assays *in vitro*, these factors were possibly concentrated into higher values in the limited areas where tumor cells closely contact with adjacent stromal cells that produce these factors.

Previous reports suggested that Fgf1 and Fgf2 bind with high affinity to Fgfr1c, 2b, 2c, and 3c and Fgfr1c and 2c, respectively (23). Immunohistochemical staining for Fgfrs revealed that Fgfr1 and 3 were expressed both in tumor and stromal cells, and Fgfr2, which was thought to be a mesenchymal Fgfr2c isofom, was strongly positive in stromal cells compared with tumor cells (Fig. 4B). These findings were largely compatible with the gene expression patterns (Fig. 4C). Interestingly, the gene expression levels of Fgfr2 and 3 were different between AX cells and those sorted from tumors. These results might reflect to the altered response of AX cells to the ligands after tumor development *in vivo*. In addition, the immunohistochemical staining of Fgfr1 indicated that the expression level of Fgfr1 in the fibroblasts surrounding the tumors was variable (Fig. 4B), which might be the cause of a large error bar of *Fgfr1* expression in the sorted fibroblasts (Fig. 4C). It is possible that fibroblasts surrounding tumors contain heterogeneous populations which play different roles responding to the ligands.

To investigate the mechanisms underlying the suppression of osteogenesis by Fgf2, we conducted real-time RT-PCR analyses of AX cells cultured in osteogenic medium supplemented with Fgf2 and evaluated the expression levels of genes that are involved in osteogenesis. The expression of all osteogenic genes examined, including *Runx2*, *Sp7*, *Alp*, *Bglap1*, and *Ibsp*, was downregulated after 4 days' culture supplemented with Fgf2 compared with those in osteogenic medium alone (Fig. 4D). Notably, the downregulated expression of osteogenic genes could be reverted by withdrawal of Fgf2 from the conditioned medium in a time-dependent manner. These results suggested that the suppression of osteogenesis by Fgf2 was reversible in AX cells and that, after the cancellation of the Fgf2 effect, the osteogenic process in osteosarcoma tumors could be restored to the previous levels. Nuclear Runx2 was strongly positive inside the tumors, whereas it was negative at the peripheral Fgf2-rich areas (Fig. 4E), suggesting that the suppression of osteogenic gene expressions by Fgf2 could also occur *in vivo*.

FGF2 inhibits osteogenesis in a human osteosarcoma cell line

Next, we investigated the effects of FGF2 on human osteosarcoma cell lines including U2OS, SAOS2, and SJSA1. Growth of these 3 cells was slightly enhanced by the treatment with FGF2, although the effect was modest compared with AX cells (Fig. 5A). Whereas U2OS and SJSA1 did not show any osteogenic differentiation, SAOS2 exhibited osteogenesis which was suppressed by FGF2 treatment similar to AX cells (Fig. 5B). In addition, the gene expression levels of osteogenic markers were attenuated by FGF2 in SAOS2 and U2OS cells (Fig. 5C). The phosphorylation level of ERK1/2 was enhanced in all osteosarcoma cell lines examined (Fig. 5D). Collectively, some characteristic effects of FGF2 on our established osteosarcoma mouse model were also observed in other osteosarcoma systems.

The suppression of osteogenesis by Fgf2 in osteosarcoma was dependent on Erk1/2 phosphorylation

Fgf2 highly activates Erk1/2 (Fig. 3A) and potently suppresses osteogenesis (Fig. 2C) in AX cells *in vitro*. Immunohistochemical staining of serial sections of AX-derived osteosarcoma tumors revealed that Erk1/2 was highly activated mainly in the interfacial regions between tumors and host tissues (Fig. 6A). Because Erk1/2 was activated mainly in the regions where immature tumor cells were found, we speculated that such a hyperactivation of Erk1/2 by environmental factors might play critical roles in the suppression of osteogenesis in osteosarcoma tumor tissues.

To verify this notion, osteogenic ability under the blockade of Fgfr or Mek signaling pathways was analyzed with each inhibitor. Erk1/2 was strongly phosphorylated by treatment with Fgf2 in AX cells, within 60 minutes (Fig. 6B). Supplementation of an Fgfr inhibitor, PD173074, SU5402, or a Mek inhibitor, U0126, almost completely blocked this activation process. Another Mek inhibitor; PD98059 also suppressed the activation of Erk1/2; however, this effect was less potent. Next, whether these inhibitors could rescue the suppression of osteogenesis by Fgf2 was examined. Reflecting the potent inhibition of the Fgfr signaling pathway as shown in Fig. 6B, supplementation with SU5402 or PD173074 successfully rescued the osteogenic differentiation suppressed by Fgf2 (Fig. 6C). Treatment with DMSO alone (1:200) did not affect the osteogenic process in AX cells. The knockdown of both Fgfr1 and Fgfr2 expressions by siRNA also appeared to rescue the osteogenic differentiation suppressed by Fgf2 (Supplementary Fig. S3A and S3B). In addition, osteogenic ability blocked by Fgf2 in AX cells was restored by supplementation with U0126 (Fig. 6D). The other Mek inhibitor, PD98059, was not able to rescue osteogenesis. This appeared to reflect an insufficient level of Mek inhibition by PD98059 compared with U0126 in AX cells (Fig. 6B). Of note, AX cells did not show osteogenesis under treatment with each inhibitor alone, without osteogenic medium (data not shown). Also, importantly, the suppression of osteogenesis by Lif, which activates Erk1/2 more weakly than Fgf2 (Fig. 3A), could be restored by treatment with PD98059 (Fig. 6D). Consistent with these findings, the treatment of U0126 at a lower concentration compared with those in the Fgf2 experiment could also rescue osteogenic ability of AX cells inhibited by Lif treatment (Fig. 6D).

Next, it was further examined whether the suppression of osteogenic gene expression by Fgf2 treatment could be reverted through supplementation with Fgfr or Mek inhibitors. The expression levels of *Runx2*, *Sp7*, and *Alp*, all of which critically involve in osteogenesis, were downregulated

Published OnlineFirst on January 6, 2012; DOI:10.1158/1541-7786.MCR-11-0347

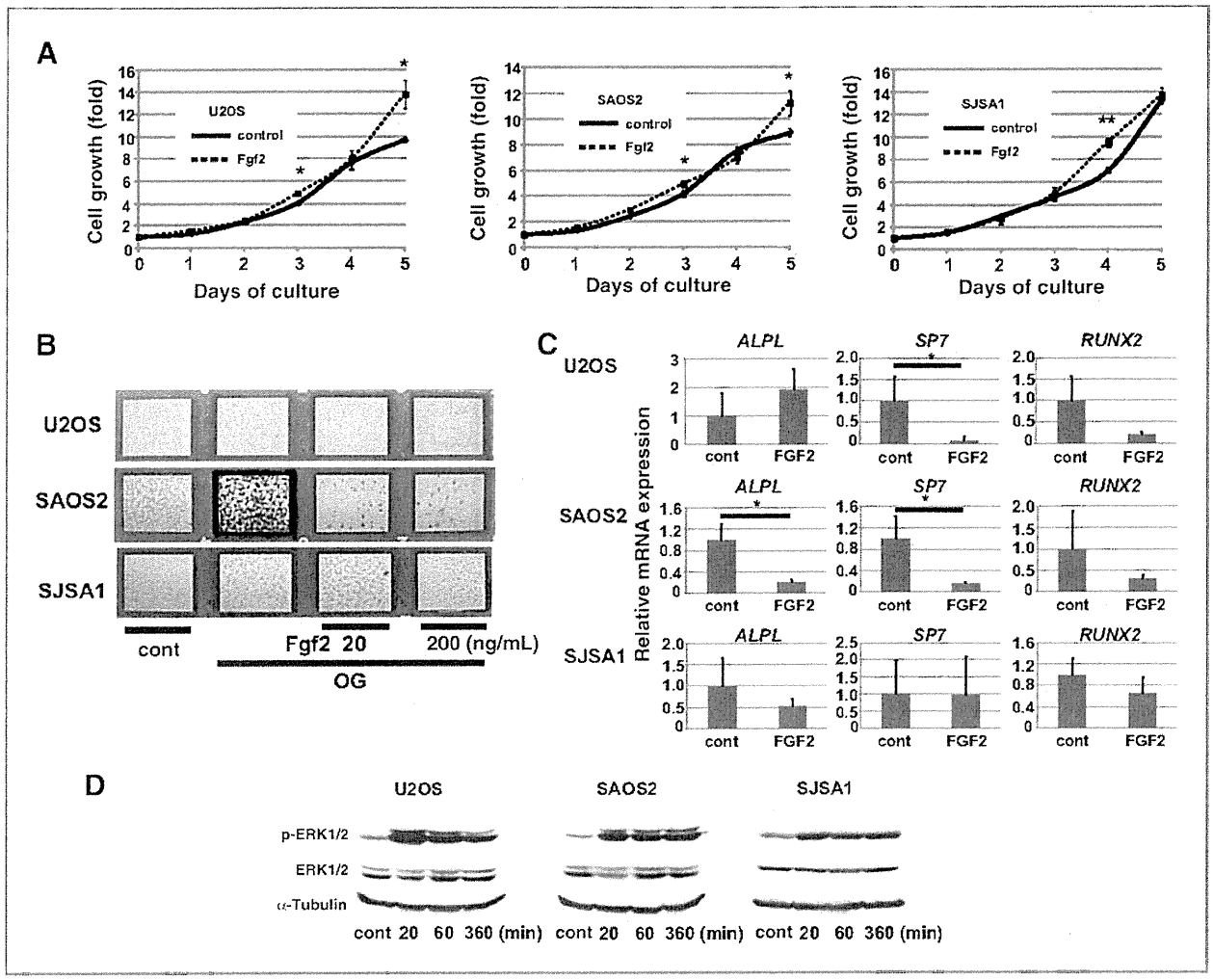

Figure 5. Fgf2 suppressed osteogenesis in human osteosarcoma cells. A, cell proliferation was analyzed with or without 20 ng/mL of FGF2. Data are shown as the ratio of the measurement of each time point to that of day 0 and represented as means ± SD from 3 independent experiments. *, $P < 0.05$; **, $P < 0.005$; NS, not significant (the Student *t* test). B, osteogenesis was evaluated by Alizarin Red S staining of cells in osteogenic medium with or without FGF2 for 14 days. OG, osteogenic culture condition. C, human osteosarcoma cells were cultured with or without FGF2 (20 ng/mL) for 1 day. The expression of osteogenic genes was assessed by real-time RT-PCR analysis. Results are shown as the ratio of the abundance of each mRNA to that of *Gapdh*. ($n = 3$). *, $P < 0.05$ (the Student *t* test). D, phospho-ERK1/2 and ERK1/2 were assessed by immunoblotting. osteosarcoma cells were treated with FGF2 (20 ng/mL) for the indicated times. α-Tubulin was used as a loading control.

upon 1 day of treatment with Fgf2 (Fig. 6E). Notably, supplementation with SU5402, PD173074, or U0126 could restore the expression of all genes. Collectively, Fgf2 suppressed the osteogenic process in AX cells at the mRNA level and the mechanism might be dependent on the hyperactivation of Erk1/2.

To further evaluate the earlier findings *in vivo*, AX cells were coinjected with Fgf2 or Lif polyhedra which were the cubic protein microcrystals continuously releasing each factor for more than 1 month (13, 14, 15). Fgf2 and Lif were successfully enriched in the surrounding areas of each polyhedra where Erk also appeared to be hyperphosphorylated (Supplementary Fig. S4A and S4B). GFP-negative fibroblastic cells proliferated in the polyhedron abundant regions. Notably, Alizarin Red S positive osteogenic differentiation was not found near around the Fgf2 or Lif polyhedra (Fig. 6F; Supplementary Fig. S4B). These findings suggest that Fgf2 and Lif also hyperactivate Erk1/2 and suppress osteogenesis of osteosarcoma cells *in vivo* as well.

Fgf2 enhanced the motility of AX cells and afforded chemoresistance

As shown in the earlier analyses, environmental factors promoted cellular proliferation and suppressed osteogenic differentiation of osteosarcoma cells. The impacts of these factors on osteosarcoma tumor progression were further assessed.

At first, cellular motility was evaluated by Transwell migration assays with Transwell membrane filter inserts (24, 25). Although AX cells exhibited high basal levels of

Published OnlineFirst on January 6, 2012; DOI:10.1158/1541-7786.MCR-11-0347

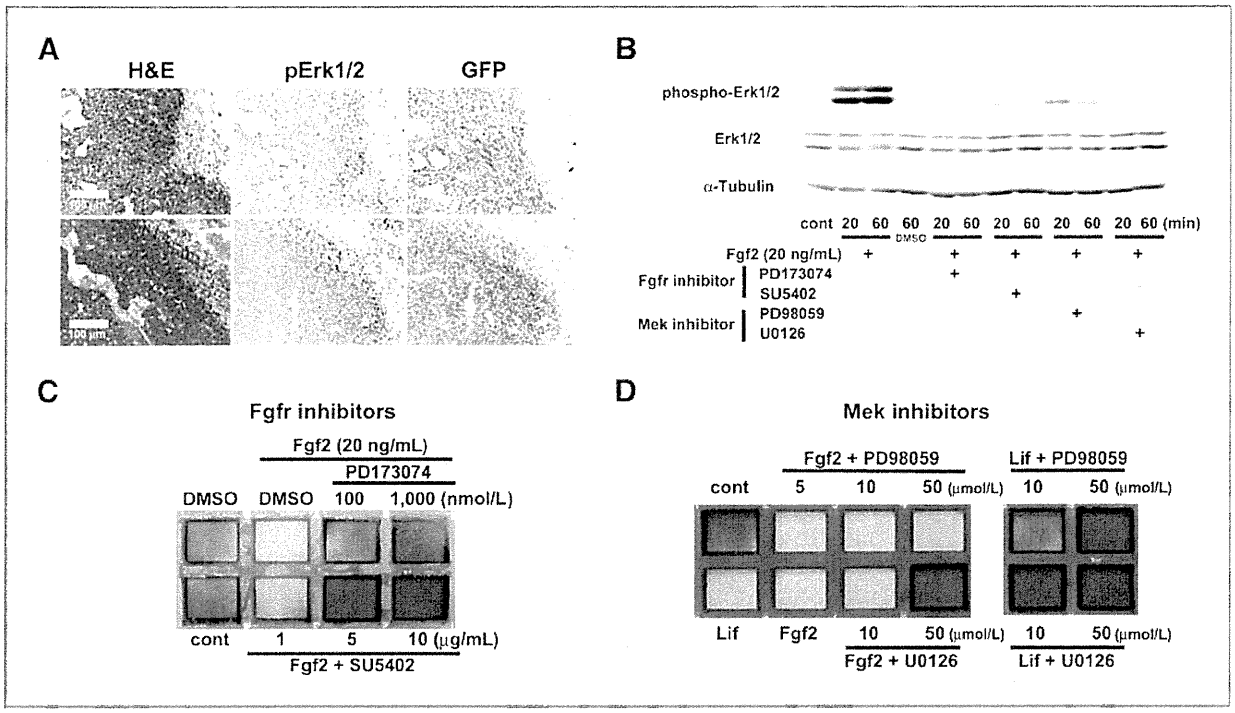

Figure 6. Osteogenesis in AX cells was rescued by the inhibition of Erk1/2 phosphorylation. A, immunohistochemistry of serial sections of an AX-derived osteosarcoma tumor for phospho-Erk1/2. Tumor cells were identified by GFP positivity. B, AX cells were cultured under osteogenic medium supplemented with or without Fgf2 (20 ng/mL), Fgfr inhibitors (SU5402, 10 μg/mL; PD173074, 1 μmol/L), or Mek inhibitors (U0126, 50 μmol/L; PD98059, 50 μmol/L) for the indicated times. Phosphorylation of Erk1/2 was assessed by Western blotting. α-Tubulin was used as a loading control. C, osteogenesis was evaluated by Alizarin Red S staining of AX cells in osteogenic medium supplemented with or without Fgf2 (20 ng/mL) or Fgfr inhibitors (SU5402 or PD173074) at the indicated concentrations for 7 days. D, osteogenesis was evaluated by Alizarin Red S staining of AX cells in osteogenic medium supplemented with or without Fgf2 or Mek inhibitors (PD98059 or U0126) at the indicated concentrations for 7 days. Suppression of osteogenesis by Lif (2,000 U/mL) in AX cells was also assessed by the same method.

motility, with more than 300 cells migrating through Transwell filters over 4 hours, this motility was enhanced to levels 1.5 times that of the basal level in the presence of Fgf2 (Fig. 7A and B). Given that the proliferative effect due to cell division could be ignored in a 4-hour observation period (data not shown), the enhancement of cell motility by Fgf2 was significant. Supplementation with Lif or Igf1 also tended to promote cellular motility (Fig. 7B). Notably, the motility was significantly enhanced with the combined treatment of these factors compared with that of each factor alone. The invasion ability of AX cells was not enhanced in the presence of Fgf2 or Lif, although both factors showed a slight tendency to enhance the invasion ability of AX cells (data not shown). These findings indicated that Fgf2 could also affect the cellular motility of osteosarcoma cells.

Finally, the influence of Fgf2 on the chemotherapeutic treatment of osteosarcoma cells was examined because previous reports suggested that Fgfr signaling affects the sensitivity of anticancer agents (20, 26, 27). Adriamycin is a well-known agent for osteosarcoma treatment and is commonly combined with several other chemotherapeutic agents (1). Cell proliferation assays under treatment with Adriamycin revealed that supplementation with Fgf2 slightly but significantly attenuated the cytotoxic effect of Adriamycin up to 80 ng/mL compared with that in control cells. (Fig. 7C). To further evaluate whether Fgfr signaling pathway could be a potential target for osteosarcoma, a combined treatment of the Fgfr inhibitor (PD173074) together with Adriamycin was conducted *in vivo*. Treatment of PD173074 or Adriamycin alone did not exhibit any antitumor effect (Fig. 7D and E). However, primary tumors in mice treated with both PD173074 and Adriamycin were significantly smaller than those in control mice or mice treated with each single agent. All tumors equally exhibited mineralized mature bone formation (Supplementary Fig. S5). Tumors in mice treated with a combination of PD173074 and Adriamycin appeared to have more osteoid formation even at the peripheral part of tumors compared with other groups (Fig. 7F). Osteogenic differentiation process might be enhanced by the combination therapy. In contrast, treatment with PD173074 or Adriamycin alone did not show any apparent microscopic difference. Therefore, although the combined treatment could not cease the primary tumor growth or metastatic process (data not shown), the inhibition of Fgfr signaling might be effective in terms of the sensitization of osteosarcoma cells to conventional chemotherapies *in vivo*. Collectively, these results indicated that Fgf2 moderately contributes to the enhancement of cellular motility and the reduction of